THE PARTIAL OXIDATION OF UNSATURATED HYDROCARBONS WITH H$_2$O$_2$ OVER TS-1 INVESTIGATED BY ONIOM METHOD: FORMATION OF ACTIVE SITE AND REACTION MECHANISM

INTRODUCTION

Zeolite is a heterogeneous catalyst which is widely used for environmental and industrial applications (Van Santen and Kramer, 1995). Various chemical processes take advantage of the high activity of inserted transition metal atoms, for example Al and Ti, in the MFI framework. Titanium silicalite-1, TS-1 (Taramasso *et al.*, 1983), is one of the most important catalysts extensively used in the chemical industry due to its very high catalytic activity and selectivity in oxidation reactions. Moreover, Ti-containing siliceous nanoporous and mesoporous materials have been found to exhibit a great performance in mild oxidation reactions in the presence of hydrogen peroxide for various organic compounds, for instance, the epoxidation of unsaturated hydrocarbons, the conversion of ammonia to hydroxylamine, the oxidation of alkanes, amines, alcohols, the hydroxylation of aromatic compounds and ketones ammoximation (Bellussi *et al.*, 1992; Bengoa *et al.*, 1998; Clerici *et al.*, 1991; Khouw *et al.*, 1994; Kumar and Bhaumik, 1998; Mantegazza *et al.*, 1996; van der Pol and van Hooff, 1993; Zecchina *et al.*, 1996).

In spite of the fact that TS-1 and silicalite-1 have the same MFI-type structure, only TS-1 shows the catalytic activity in oxidation. Theoretical and experimental studies showed evidences that the Ti atom in the crystal lattice is the most probable active center in facilitating the catalytic oxidation process (Barker *et al.*, 2002; Barker *et al.*, 2001; Bonino *et al.*, 2004; Bordiga *et al.*, 2003; Damin *et al.*, 2002; Lamberti *et al.*, 2001; Sankar *et al.*, 2001; Sever and

Root, 2003a, b; Sinclair and Catlow, 1999; Sinclair *et al.*, 1997; Tozzola *et al.*, 1998; Zecchina *et al.*, 1996; Zhuang *et al.*, 2004). Therefore, the occupying detail of Ti atoms in the TS-1 framework becomes an important point for understanding the structure and catalytic activity. Unfortunately, the trace amount of titanium atoms made difficult to determine how they distribute among the 12 crystallographically distinct T sites for last two decades. Recently, many efforts have been devoted to observe the preferential sites of Ti in the TS-1 framework. The results revealed that the distribution of Ti atoms in the MFI framework is non-random but their favored sites are sensitive to the synthesis conditions (Atoguchi and Yao, 2003; Henry *et al.*, 2001; Hijar *et al.*, 2000; Lamberti *et al.*, 2001).
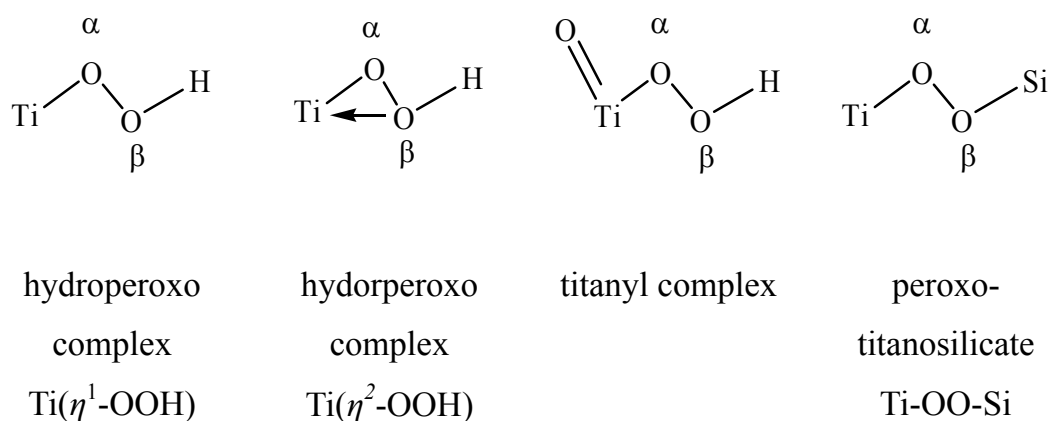

| hydroperoxo complex $Ti(\eta^1\text{-OOH})$ | hydorperoxo complex $Ti(\eta^2\text{-OOH})$ | titanyl complex | peroxo-titanosilicate Ti-OO-Si |

Figure 1 Proposed oxidative active species in the catalytic epoxidation reaction of unsaturated hydrocarbons with H_2O_2 over TS-1. The arrow represents the coordinative interaction.

Many active species, including titanium hydroperoxo complexes, in mono- and bi-dentate manners, and titanyl form (Figure 1) have been proposed for mild epoxidation processes catalyzed by H_2O_2 and TS-1 (Barker *et al.*, 2001; Clerici *et al.*, 1991; Karlsen and Schoeffel, 1996; Khouw *et al.*, 1994;

Limtrakul *et al.*, 2004; Lin and Frei, 2002; Mantegazza *et al.*, 1999; Perego *et al.*, 2001; Sankar *et al.*, 2001; Sever and Root, 2003a, b; Sinclair and Catlow, 1999; Tantanak *et al.*, 1998; Tozzola *et al.*, 1998; Vayssilov and Van Santen, 1998; Wells *et al.*, 2004; Yudanov *et al.*, 1999). However, the diffuse refractance UV-vis (UV-vis DRS) spectra contained no information regarding the titanyl species (Boccuti *et al.*, 1989). Computational studies of small clusters without solvent molecules have shown that the bi-dentate titanium hydroperoxo complex, $Ti(\eta^2\text{-OOH})$, was the most energetically favorable active species. It has been used as an active site for the epoxidation reaction of ethylene on the titanium silicalite-1 (Limtrakul *et al.*, 2004). Nevertheless, when two water molecules were included in the model, the mono-dentate form, $Ti(\eta^1\text{-OOH})$, was preferred (Sankar *et al.*, 2001). Wells *et al.* (Wells *et al.*, 2004) have proposed that $Ti(\eta^1\text{-OOH})$ was the active species for propylene epoxidation. They found that the introduction of Ti located near Si vacancy sites facilitated the active site formation. An additional active species known as the peroxo-titanosilicate, Ti-O-O-Si (Figure 1), was recently proposed by Munakata and co-workers (Munakata *et al.*, 2001). However, this active species was highly unstable when using the constraint model.

To our knowledge, only small cluster models were used for studying the mechanism of the active site formation, stability, and catalytic activity in epoxidation. Thus, some reaction pathways, which may have a lower barrier, are not able to be located by using such small models. To better understand the reaction mechanism in the real zeolite pores, it is essential that the effect of the lattice framework be included. Several theoretical models, together with the periodic structure calculations, have been proposed to study the interactions in extended systems of crystals or surfaces (Dungsrikaew *et al.*, 2003; Jeanvoine and Angyan, 1998; Ketrat and Limtrakul, 2003; Limtrakul *et al.*, 2001b; Sauer and Sierka, 2000; Shah *et al.*, 1997; Teunissen *et al.*, 1994; Treesukol *et al.*,

2001). For nanostructured materials, for example zeolites, that have a great potential in industrial processes usually possess hundreds of atoms per unit cell. This makes the use of accurate periodic structure calculations computationally too expensive and even impractical when very large zeolites are concerned. However, embedded cluster or combined Quantum Mechanics/Molecular Mechanics (QM/MM) methods (Greatbanks *et al.*, 1996; Hillier, 1999; Khaliullin *et al.*, 2001; Limtrakul *et al.*, 2000; Limtrakul *et al.*, 2001a; Sauer and Brandle, 1998; Sinclair *et al.*, 1998), the more general Our-own-N-layered Integrated molecular Orbital/molecular Mechanics (ONIOM) method (Svensson *et al.*, 1996) have brought a larger system within reach of obtaining accurate results. The ONIOM scheme based on the integration of the molecular orbital at different levels of theory, has been validated in many zeolite systems for predicting the adsorption energy, activation barrier as well as the optimized structures due to its low computational demand (Atoguchi and Yao, 2003; Bobuatong and Limtrakul, 2003; Boronat *et al.*, 2004; Damin *et al.*, 2002; Jiang *et al.*, 2004; Kasuriya *et al.*, 2003; Namuangruk *et al.*, 2004; Panjan and Limtrakul, 2003; Raksakoon and Limtrakul, 2003; Rungsirisakun *et al.*, 2004; Sillar and Burk, 2004; Solans-Monfort *et al.*, 2002; Solans-Monfort *et al.*, 2005).

In the present work, we intensively investigated on the reaction mechanisms of the oxidative active site formation and the epoxidation of unsaturated hydrocarbons. The Ti active center located adjacent to the Si vacancy site was modeled as the TS-1 active site. This model is sufficient to study two different competing reaction channels for the oxidative active site formation. The stability of oxidative active species in different configurations and in the presence of water molecules is also discussed. Finally, the effect of molecular chain length on the partial oxidation of small olefins, including ethylene, propylene and *trans*-2-butylene, by TS-1 and H_2O_2 were examined. In

order to include the confinement effects by the zeolite framework, the ONIOM method that takes advantage of the density functional theory for the accurate treatment of the interactions of reactive intermediates with the Ti site in the crystal framework of TS-1 and of the Universal Force Fields (UFF) for manifestation of the van der Waals interaction due to the confinement of the extended zeolite structure, was adopted to evaluate the energy profile throughout the reaction mechanisms in this study.

LITERATURE REVIEW

Zeolite is one of the most important heterogeneous catalysts intensively used in industry. They can be found naturally as a component of certain clays or synthesized in the laboratory, for example, MFI, TS-1, and MCM. In 1983, Taramasso (Taramasso *et al.*, 1983) has discovered titanium silicalite-1 (TS-1) by the insertion of Ti atom into the siliceous MFI-type zeolite framework. This makes TS-1 remarkable as high competent and selective catalyst in oxidation reactions employing hydrogen peroxide (H_2O_2). Its structure and applications have been extensively investigated by both computational and experimental studies. The distribution of titanium atoms among distinguishable 12 T sites is still debate. The X-ray diffraction data suggested a random substitution of Ti among the 12 crystallographically distinct Si sites in the framework of TS-1. However, the high resolution of powder neutrons diffraction technique recommended that the preferential sites of Ti may be located at sites T3, T7, T8, T10 and T12 (Hijar *et al.*, 2000). The incorporation of titanium into the zeolite framework can be directly achieved by the hydrothermal synthesis or by the post-synthesis treatment with $TiCl_4$. The latter treatment also showed the non-random preferential sites of titanium atoms in the zeolite framework. By using the well-manufacture TS-1 sample from the EniChem Novara and the neutron powder diffraction study, Lamberti *et al.* (Lamberti *et al.*, 2001) found the strong evidence of the preferential sites of non-random titanium atoms substituted on the framework located at sites T6, T7 and T11 and weak evidence on T10 from distinguishable 12 T sites. These sites are the positions of the Si vacancy sites found in defective silicalite reported in their previous work (Artioli *et al.*, 2000). Therefore, the mechanism of incorporating titanium atoms into the MFI framework may occur via the insertion of titanium atoms into the vacancy sites of defective orthorhombic silicalite. In addition, Henry *et al.* (Henry *et al.,* 2001) presented constant wavelength powder neutron

diffraction data collected on isotopic TS-1 samples. Their information showed that both titanium occupying and silicon vacancy sites are non-random. The titanium preferential sites are T3, T8 and T10 from 12 different T sites and the Si vacancy sites are T1 and T5.

Recently, Atoguchi et al. (Atoguchi and Yao, 2003) have performed computational study on the relative stability between T sites of titanium atom sitting in the MFI framework of a large cluster model containing about 200 atoms trimmed from MFI zeolite crystal. The silicon atoms were replaced by titanium atoms at 12 distinct T sites resulting in different $Ti(OSi)_4$ sites, which were optimized for locally relaxed geometry by using the ONIOM (B3LYP/LANL2DZ:UFF) method. The single-point energies of the optimized structures were performed by means of the ONIOM (B3LYP/LANL2DZ:B3LYP/LANL2MB) method. The calculated results suggested that most thermodynamically stable sites for titanium sitting on the MFI framework are sites T9 and T10. The titanium atoms also may be incorporated among T1, T3, T5, T6 and T12 sites, while the others are unstable sites.

As mentioned previously, Ti-containing siliceous nanoporous and mesoporous materials have been found to exhibit excellent performance in mild oxidation reactions in the presence of hydrogen peroxide for various organic compounds, for instance, the epoxidation of unsaturated hydrocarbons, the conversion of ammonia to hydroxylamine, the oxidation of alkanes, amines, alcohols, the hydroxylation of aromatic compounds and ketones ammoximation (Bellussi *et al.*, 1992; Bengoa *et al.*, 1998; Clerici *et al.*, 1991; Karlsen and Schoeffel, 1996; Khouw *et al.*, 1994; Kumar and Bhaumik, 1998; Mantegazza *et al.*, 1996; van der Pol and van Hooff, 1993; Zecchina *et al.*, 1996). Several active species of hydrogen peroxide upon the titanium atoms have been proposed to play a key role in partial oxidation of olefin and ammonia. The

most famous active species is a Ti-hydroperoxo complex (Barker *et al.*, 2002; Barker *et al.*, 2001; Mantegazza *et al.*, 1999; Perego *et al.*, 2001; Sankar *et al.*, 2001; Sinclair and Catlow, 1999; Tantanak *et al.*, 1998; van der Pol and van Hooff, 1993; Vayssilov and Van Santen, 1998) in bi-dentate (η^2) and mono-dentate (η^1) manners (see Figure 1). Although these species have been suggested to play an important role in the partial oxidation mechanism, the other form, peroxo and superoxo, can not be ruled out. Sinclair et al. (Sinclair and Catlow, 1999) performed density functional theory (DFT) calculations on a titanium cluster and showed that the short lived titanyl group could be formed in protic solvents as shown in Figure 1. Nevertheless, the diffuse refractance UV-vis (UV-vis DRS) spectra contained no information regarding this titanyl species (Boccuti *et al.*, 1989). Experimental and theoretical studies in the presence of solvent molecules (Sever and Root, 2003b), show that the coordination number of the titanium center expands from four to five or six due to the interaction of small molecules of solvents with electrons acceptor at the Ti center (Barker et al., 2002). The computational studies of small clusters without solvent molecules showed that the bidentate titanium hydroperoxo complexes are the most energetically favorable active species (Lamberti et al., 2001; Munakata et al., 2001; Perego et al., 2001; Tantanak et al., 1998). However, Tozzola et al. (Tozzola et al., 1998) found the monodentate form in the same cluster when two water molecules were included in the model. Sankar et al. (Sankar et al., 2001) combined in situ extended X-ray adsorption fine structure (EXAFS) and DFT calculations to study the active species of Ti↑MCM-41. The results supported that the Ti(IV) active of Ti↑MCM-41 have octahedral coordinates during the epoxidation of alkenes. By using an in situ probe reaction of trimethyl phosphene ($^{31}P(CH_3)_3$) or TMP with the solid-state MAS NMR technique, Zhuang et al. (Zhuang et al., 2004) found that the TMP distorted tetrahedral-coordinated titanium species in the framework of zeolite and the coordinated-unsaturated Ti(IV). They proposed that the active centers

of TS-1 were Ti atoms because they would be able to accept the electrons transferred from the probe molecules (TMP). The results from ^{31}P MAS NMR spectra showed that the adsorbed TMP at the Ti center is more reactive than at the other Lewis acid sites.

Barker and Munakata performed DFT calculations of the formation of the active species on the cluster model of titanosilicate catalyst in the absence of solvent molecules. Barker et al. (Barker et al., 2001) calculated the activation energy for H transfer from H_2O_2 to OH of the Ti(OSi)$_3$OH cluster to form the Ti(OSi)$_3$OOH.H_2O active complexes. They found that the activation barriers for bidentate and monodentate intermediate were 9.1 and 11 kcal/mol, respectively. Munakata and co-workers (Munakata et al., 2001) showed the hydrated peroxo (Ti-O-O-Si) complexes (Figure 1) were the active species. This was established via the proton transfer from the hydrogen peroxide to oxygen framework of the zeolite, resulting in the rupture of Ti-O-Si bridging. The hydrated peroxo complex was produced subsequent to the collapse of the Si-OH and Ti-OOH groups. They also demonstrated the mechanisms of epoxidation reaction and ammonia to hydroxylamine in which the hydroperoxo complex served as an active site. The activation barrier was calculated to be 16.5 and 13.9 kcal/mol for the epoxidation and ammoximation reactions, respectively. Recently, the computational calculations and the experimental techniques, Resonant Raman spectroscopy, EXAFS and UV-vis DRS, have been applied for characterizing the mechanism of the formation and the interconversion of the active species of TS-1/H_2O_2/H_2O system by Bonino et al. (Bonino et al., 2004). The results proved that the dehydration of TS-1/H_2O_2/H_2O turned the catalyst from yellow color into colorless, and is responsible for the peroxo species (O-O bound to Ti) to the hydroperoxo species (O-OH bound to Ti) respectively. According to the two active species having different oxidizing ability, water might be expected to play an important

role in partial oxidation reactions. Limtrakul et al. (Limtrakul et al., 2004) reported DFT calculations of the mechanism of the active site formation and epoxidation reaction on the cluster of titanium silicalite-1 and embedded cluster in a set of point charges, generated by the surface charge representation of external embedded potential method (SCREEP). They found that the Ti(η^2–OOH) complex was the active species and the inclusion of the zeolite crystal framework was the crucial point for increasing the barrier of oxygen transfer step by 5.0 kcal/mol. Wells et al. (Wells *et al.*, 2004) have performed the density functional theory study of hydroperoxo intermediates on the non-defect and defect TS-1 models and showed that Ti sites located adjacent to Si vacancies in the TS-1 lattice were more reactive in propylene epoxidation than fully coordinated Ti sites, which they found do not react at all. They proposed that the propylene epoxidation near a Si-vacancy occurs through a sequential pathway where H_2O_2 first form a monodentate hydroperoxo intermediate with the activation barrier of 15.4 kcal/mol and then reacted with propylene by the proximal oxygen abstraction (O_α) with the activation energy of 9.3 kcal/mol. They used the terminated clusters to model the active site in TS-1 for both the defect and non-defect cases and the substituted Ti atom was placed at the T6 site in the 12 different tetrahedral sites in the orthorhombic structure of TS-1 according to the finding of Lamberti et al. (Lamberti *et al.*, 2001) that 5-8 % of T sites in the well-made TS-1 are defective. Furthermore, a Ti-substituted site, which locates inside the crystallographic lattice nearby a Si vacancy site, has significantly different properties from non-defect Ti sites and surface Ti sites, where it has neighboring silanol groups to coordinate with reactant ligands and its activity must be different also.

MATERIALS AND METHODS

1. Density Functional Theory (DFT)

The ground state energy is given as

$$E_0 = \overline{T}[\rho] + \overline{V}_{Ne} + \overline{V}_{ee}[\rho] \tag{1}$$

where $\overline{T}[\rho]$ is the electronic kinetic energy and $\overline{V}_{Ne}$, $\overline{V}_{ee}[\rho]$ are the electron-nuclear attraction and electron-electron repulsions. Kohn and Sham considered a fictitious reference system in which the electrons in system do not interact each other, therefore, the Hamiltonian of the reference system is

$$H_s = \sum_{i=1}^{n}\left[-\frac{1}{2}\nabla_i^2 + v_s(r_i)\right] \tag{2}$$

where $v_s(r_i)$ is the external potential function to make the ground-state electron probability density of reference system equal to the exact ground-state electron density of the molecule we are interested.

The basic idea in the Kohn and Sham (KS) formalism is to split the kinetic energy functional into two parts, one of which can be calculated exactly, and the other small correction term to solve the main problem of poorly represented kinetic energy in Thomas-Fermi models. For a closed shell ground state, the electrons are paired in the Kohn-Sham orbitals, with two electrons of opposite spin having the same spatial Kohn-Sham orbital. Kohn and Sham rewrote the equation (1) as follows: Let $\Delta\overline{T}[\rho]$ be defined by

$$\Delta\overline{T}[\rho] = \overline{T}[\rho] - \overline{T}_s[\rho] \tag{3}$$

where $\Delta \overline{T}[\rho]$ is the difference in the average ground-state electronic kinetic energy between the molecule and the reference system of non-interacting electrons with the electron density equal to that in the molecule.

$$\Delta \overline{V}_{ee}[\rho] = \overline{V}_{ee}[\rho] - \frac{1}{2} \iint \frac{\rho(r_1)\rho(r_2)}{r_{12}} dr_1 dr_2 \qquad (4)$$

where r_{12} the distance between points x_1, y_1, z_1 and x_2, y_2, z_2. The $\frac{1}{2} \iint \frac{\rho(r_1)\rho(r_2)}{r_{12}} dr_1 dr_2$ is the classical expression for the electrostatic inter-electronic repulsion energy. The equations (1), (3) and (4) thus become

$$E_0[\rho] = \overline{V}_{Ne} + \overline{T}_s[\rho] + \overline{V}_{ee}[\rho] + \frac{1}{2} \iint \frac{\rho(r_1)\rho(r_2)}{r_{12}} dr_1 dr_2 + E_{xc}[\rho] \qquad (5)$$

where $E_{xc}[\rho]$ is the exchange-correlation energy which is equal to $\overline{T}[\rho] + \overline{V}_{ee}[\rho]$. The $E_{xc}[\rho]$ part is the remaining part after subtraction of the non-interacting kinetic energy, and the $\overline{V}_{Ne}[\rho]$ and the electrostatic inter-electronic repulsion energy terms. If the exact $E_{xc}[\rho]$ is known, the DFT would provide the exact total energy, including the electron correlation. The hybrid exchange-correlation functionals are widely used to solve the $E_{xc}[\rho]$ value. For example, the B3LYP is the hybrid functional, which is defined by

$$E_{xc}^{B3LYP} = (1 - a_0 - a_x)E_x^{LSDA} + a_0 E_x^{exact} + a_x E_x^{B88} + (1 - a_c)E_c^{VWN} + a_c E_c^{LYP} \qquad (6)$$

where E_x^{LSDA}, E_x^{exact} and E_x^{B88} are the LSDA (Local Spin Density Approximation) exchange energy, the Hartree-Fock exchange energy and the B88(Beck's 1988) exchange energy, respectively. The terms E_c^{VWN} and E_c^{LYP}

are the VWN (Vosoko-Wilk-Nusiar) correlation energy and the LYP (Lee-Yang-Part) correlation energy.

2. __ONIOM Method__

2.1 ONIOM energy

In the two-layered ONIOM (Our-own-N-layered Integrated molecular Orbital/molecular Mechanics) method, the total energy of the system is obtained from three independent calculations:

$$E^{ONIOM2} = E^{high}_{model} + E^{low}_{real} - E^{low}_{model} \qquad (7)$$

where *real* denotes the full system, which is treated at the *low* level, while model denotes the part of the system of which the energy is calculated at both the *high* and *low* level. The concept of the ONIOM method is represented schematically in Figure 1. One can see that the method can be regarded as an extrapolation scheme. Starting from E^{low}_{model} the extrapolation to the high-level calculation $\left(E^{high}_{model} - E^{low}_{model}\right)$ and the extrapolation to the real system $\left(E^{low}_{real} - E^{low}_{model}\right)$ are assumed to give an estimate for E^{high}_{real}.

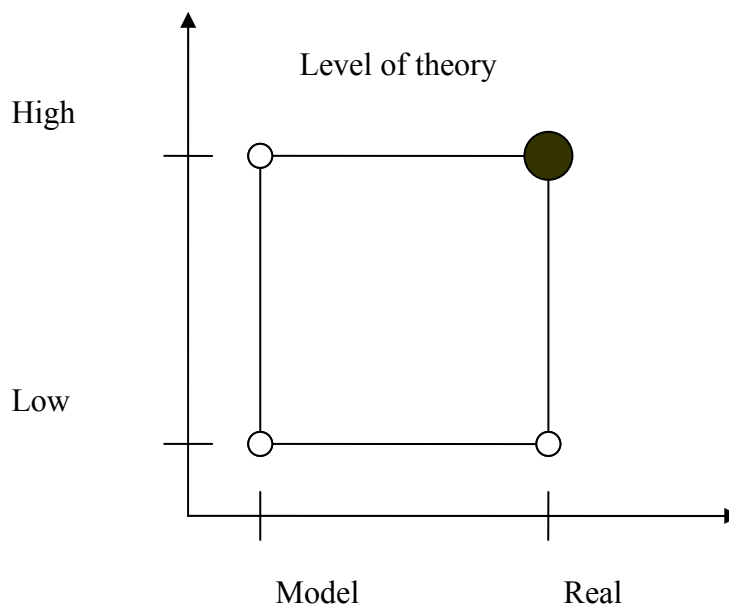High

Low

Level of theory

Model   Real

Figure 2   Schematic representation of the two-layered ONIOM extrapolation scheme.

E^{ONIOM2} is an approximation of the true energy of the real system E_{real}^{high} :

$$E_{real}^{high} = E_{ONIOM2} + D \qquad\qquad (8)$$

Thus, if the error D of the extrapolation procedure is constant for two different structures (e.g. between the reactant and transition state), their relative energy ΔE_{real}^{high} will be evaluated correctly by using the ONIOM energy ΔE_{ONIOM2}.

2.2 Treatment of link atoms

The definition of the model system is straightforward when there is no covalent bond between the layers. If one considers a solute molecule solvated with one solvent molecule as the *real* system, the solute will be the

model system, and the solute-solvent interaction is included in the *low* level calculation of the real system. However the situation becomes more complicated when a covalent bond exists between the layers. The calculation on the real system does not pose any problems, but the question is "what can be used as a model system?" Simply cutting the bonds would result in a model system with dangling bonds, and its electronic structure would be very different from the real system. The most straightforward way to ensure that the model system is representative for the real system is to saturate the dangling bonds with *link atoms*, which is the scheme chosen for ONIOM methods. For example, if a methy1 group is treated at the low level, this group can be substituted by a hydrogen atom in the model system. Link atoms should be chosen that best mimic the substituted ones that exist only in the real system. In practice, hydrogen atoms are good link atoms when carbon-carbon bonds are broken, but in some cases other atoms may be preferable.
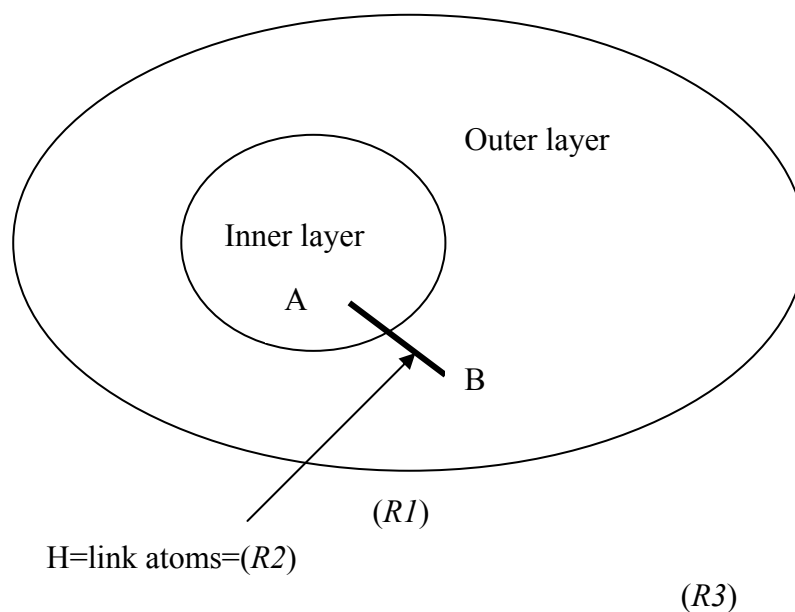
Figure 3 Definition of different atoms within the ONIOM scheme.

Where *R1*, *R2*, *R3* are a coordination of atoms in the model system, link atoms and the real system. To define *R2* as a function of *R1* and *R3*:

$$R2 = f(R1, R3) \tag{9}$$

The explicit functional form of the *R2* decency can be chosen arbitrarily. To consider the fact that link atoms are introduced to mimic the corresponding covalent bonds of the real system, they should follow the movement of the atoms they replace. To adopt the following coupling scheme: if atom A belongs to R1 and atom B belongs to *R3*, the link atom (*R2*) is placed onto the bond axis A-B. In terms of internal coordinates, the same bond angles dihedral angles are chosen for *R2* atoms as for *R3*. So, in the model calculations, the link atoms are always aligned along the bond vectors of the real system. For the exact position r_2 of a single H atom along an A-B bond $(r_3\text{-}r_1)$, to introduce a fixed scale factor (or distance parameter) *g*.

$$r_2 = r_1 + g\ (r_3\text{-}r_1) \tag{10}$$

g is constant

2.3 ONIOM gradients

The definition of the corresponding integrated gradient expression is straightforward. For a two-layered ONIOM system,

$$\nabla E_{ONIOM2} = \nabla E_3 - \nabla E_1 * J(R_2; R_1, R_3) + \nabla E_2 * J(R_2; R_1, R_3) \tag{11}$$

where *J*, the Jacobian matrix, projects the forces on all the link atoms (*R2*) onto *R1* and *R3* atoms.

3. UFF (Universal Force Field)

The parameters used to generate the Universal Force Field include a set of hybridization dependent atomic bond radii, a set of hybridization angles, van der Waals parameters, torsional and inversion barriers, and a set of effective nuclear charges.

The potential energy of an arbitrary geometry for a molecule is written as a superposition of various two-body, three-body, and four-body interactions.

The potential energy is expressed as a sum of valence or bonded interactions and nonbonded interactions:

$$E = E_R + E_\theta + E_\phi + E_\omega + E_{vdw} + E_{el} \tag{12}$$

The valence interactions consist of bond stretching (E_R). Included as angular distortions are bond angle bending E_θ, dihedral angle torsion E_ϕ and inversion

terms E_{ω}. The nonbonded interactions consist of van der Waals E_{vdw} terms and E_{el} is the electrostatic term.

4. <u>Details of calculations</u>

The defect TS-1 was modeled with two different strategies. First, the 9T quantum cluster, $TiSi_8O_{10}H_{24}$, was employed to represent the local active site whereas the second strategy was performed by partitioning the 65T cluster model, $TiSi_{64}O_{97}H_{74}$, into two levels of calculation according to the two-layer ONIOM scheme. These cluster models were obtained from the ZSM-5 zeolite lattice (Van Koningsveld *et al.*, 1987). The number of T atoms refers to tetrahedrally coordinated Ti and Si atoms in the framework model. The 65T cluster model is considered to be large enough to cover all important framework effects acting on both the active site and adsorbates. The framework structure contains a nearly circular straight channel with dimensions of 5.4×5.6 Å and a slightly elliptical zigzag channel with dimensions of 5.1×5.5 Å. Both channels intersect each other at the middle of the model and thus generating an intersecting channel with the spatial dimension of about 9 Å. The Si atom at site T5 was removed from the lattice framework to model the defect site and the neighboring Si atom at site T6 was replaced with the Ti atom to take action as the active center. These models correspond to constant wavelength powder neutron diffraction data collected on isotopic TS-1 samples which determine both titanium occupancy and silicon vacancy sites (Henry *et al.*, 2001; Lamberti *et al.*, 2001). The dangling bonds resulted from the elimination of the Si atom were terminated with hydrogen atoms. Both the 9T and 65T cluster models are illustrated in Figure 2.

Due to the limitation of computational resources and time consumption, only the small active region is usually treated accurately with the *ab initio* method, however, the effect from the framework structure of zeolite cannot be totally neglected if more accurate results are required. Therefore, in this study, the two-layered 9T/65T ONIOM scheme was adopted with the aim of imitating

the molecular properties of TS-1 and its interactions with H_2O_2 and small olefins. According to the two-layered ONIOM approach, the calculation of energies can be simplified by treating the active region with a high-level quantum mechanical (*ab initio* or density functional) approach and the extended framework environment with a less expensive level, the HF and molecular mechanics force fields. The total energy of the whole system can be expressed within the framework of the ONIOM methodology developed by Morokuma and his coworkers (Svensson *et al.*, 1996)

$$E_{ONIOM2} = E_{Low}^{Real} + (E_{High}^{Cluster} - E_{Low}^{Cluster})$$ (13)

where the superscript *Real* means the whole system and the superscript *Cluster* means the active region. Subscripts *High* and *Low* mean high- and low-level methodologies used in the ONIOM calculation. In this study, an unconstrained 9T cluster, which is referred to as "high level region", was calculated at the density functional theory with the hybrid functional B3LYP, while the rest, which is referred to as "low level region", was treated by the UFF force field to reduce computational time and to practically represent the confinement effect of the zeolite pore structure.

All calculations in this study were performed with the Gaussian03 software. The Los Alamos LANL2DZ (Hay and Wadt, 1985) effective core pseudo-potentials (ECP) and valence double-ζ basis set were used for the titanium atom and the full double-ζ basis set, 6-31G(d,p), was applied for carbon, hydrogen, oxygen and silicon atoms. During the geometry optimization, only the active 9T quantum cluster region was allowed to relax while the remainders (terminated hydrogen atoms and the environment for 9T and 65T clusters, respectively) are fixed at the lattice positions. The normal mode analyses were carried out to verify the transition states, which have only one imaginary frequency whose mode corresponds to the designated reaction

coordinate. To improve the energetic properties of the ONIOM approach, the minimized geometries of the 9T/65T ONIOM cluster scheme were used as inputs in the single point energy calculations at the same level of theory using the 30T/65T ONIOM cluster scheme.

The optimized structural parameters of the TS-1 active site model are given in Table 1. The Ti-O bond lengths are in the range of 1.753-1.802 Å and 1.773-1.855 Å for the 9T/65T ONIOM cluster and the 9T cluster, respectively, which are close to the experimental values, 1.79 Å based on XRD (Bellussi and Fattore, 1991) and 1.80-1.81 Å obtained by EXAFS, (Bordiga *et al.*, 1994; Davis *et al.*, 1995; Pei *et al.*, 1993) whereas the Ti-O1(H) bond lengths are 1.912 and 1.748 Å for the 9T/65T ONIOM cluster and the 9T cluster, respectively. The optimized TS-1 structure models using the 9T quantum cluster and the ONIOM2 scheme are shown in Figure 2, where the high level region is displayed with balls and sticks whereas the low level region is demonstrated by lines.

Table 1 Selected optimized structural parameters of TS-1 active site models using the 9T/65T ONIOM2(B3LYP/6-31G(d,p):UFF) scheme and the 9T B3LYP/6-31G(d,p) cluster.

parameter	cluster	ONIOM	Expt.
bond distance (Å)			
Ti-O1	1.830	1.912	
Ti-O2	1.802	1.820	
Ti-O3	1.788	1.760	
Ti-O4	1.765	1.753	
<Ti-O>	1.785	1.778	1.79[a], 1.80-1.81[b]
Si2-O2	1.657	1.646	
Si3-O3	1.636	1.631	
Si4-O4	1.671	1.645	
<Si-O>	1.655	1.641	
angle (°)			
∠Ti-O2-Si2	158.0	157.5	
∠Ti-O3-Si3	138.6	168.8	
∠Ti-O4-Si4	128.2	153.1	

Source: [a] (Bellussi and Fattore, 1991), [b] (Bordiga et al., 1994; Davis et al., 1995; Pei et al., 1993).

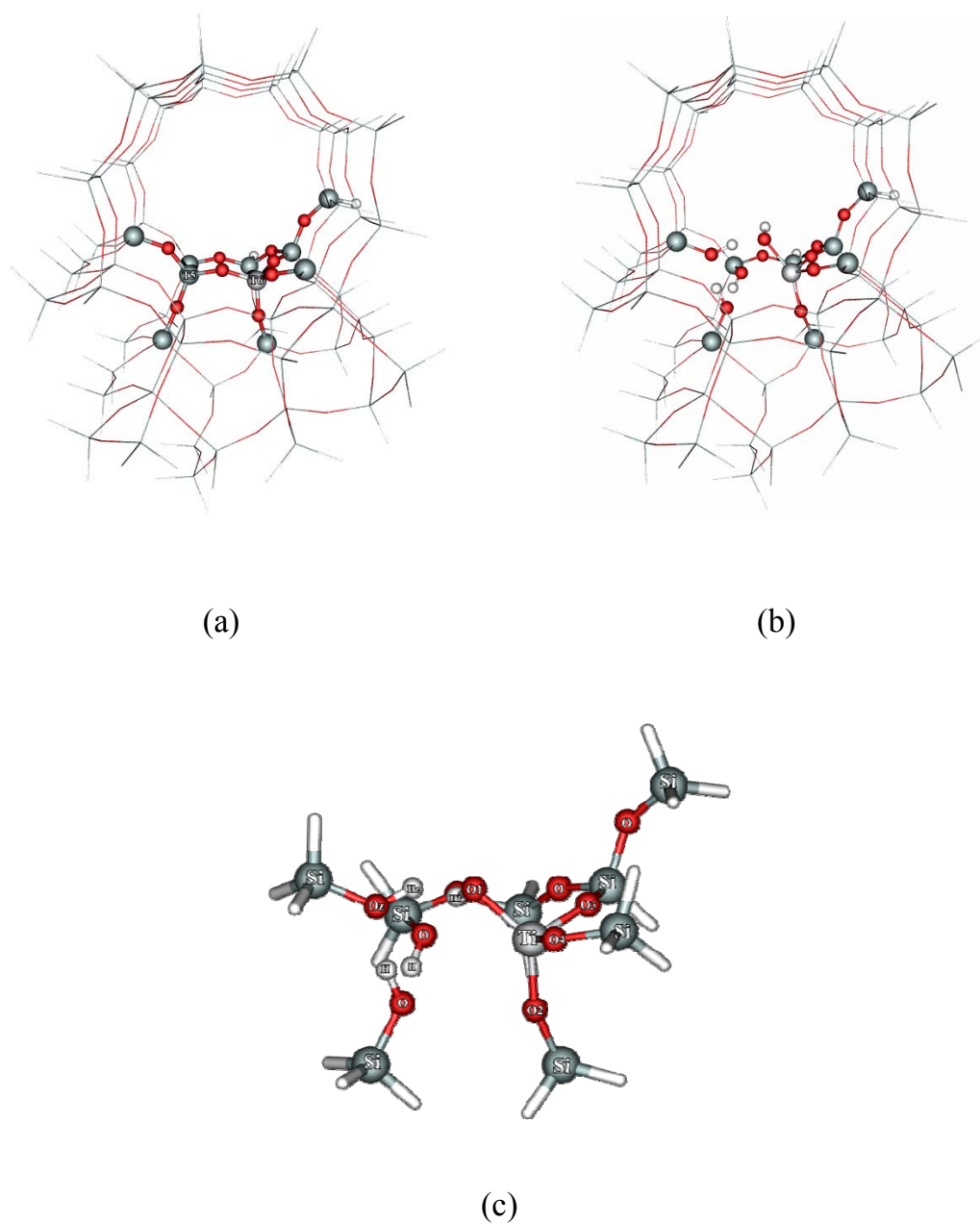(a)   (b)

(c)

Figure 4   Showing (a) two tetrahedral sites (T5 and T6) of nondefect active site and optimized structures of defect active site models using (b) the 9T/65T ONIOM2(B3LYP/6-31G(d,p):UFF) scheme and (c) the 9T B3LYP/6-31G(d,p) cluster. The high level region is displayed with balls and sticks whereas the low level region is demonstrated by lines.

RESULTS AND DISCUSSION

1. Adsorption of H_2O_2 on the Ti- substituted active site

After a H_2O_2 molecule is introduced to the defect active site of TS-1, it interacts with the substituted Ti active center via one (O_α) of the two O atoms (O_α and O_β) as shown in Figures 5-7. The interaction between O_α and the Ti center resembles a coordinative bond with a Ti$\cdots O_\alpha$ distance of 2.378 and 2.345 Å for the ONIOM2 and 9T cluster, respectively. In addition to this interaction, the H_2O_2 molecule can also form two H-bonds with the local active site O atoms through its H atoms (H_α and H_β). One is a strong H-bond between H_α and a silanol Oz atom (Oz$\cdots H_\alpha$ = 1.618 Å vs 1.502 Å) while the other is only a weak interaction between H_β and an O4 atom of the TS-1 framework (O4$\cdots H_\beta$ = 1.904 Å vs 1.776 Å). As a result of the insertion of H_2O_2, the geometrical parameters of both the active site and the adsorbing molecule are distorted from the bare geometries. The Ti-O(Si) bond, averaged over the three O framework atoms, is elongated by 0.022 vs 0.01 Å whereas the titanol Ti-O1 bond is lengthened by 0.013 vs 0.020 Å. The O-O bond of the H_2O_2 molecule undergoes a shortening by 0.015 vs 0.016 Å (from 1.456 Å to 1.441 vs 1.440 Å), while the O-H bond distance is split from 0.970 Å, an equivalent value of the bare H_2O_2, to 1.008 and 0.978 Å (vs 1.024 and 0.984 Å) for the O_α-H_α and O_β-H_β bond distances, respectively. The longer O-H bond distance of H_2O_2 in the adsorption complex refers to the stronger H-bond formation. All selected parameters of the physisorbed TS-1/H_2O_2 complex are documented in Table 2. When focusing on the geometry of the Ti active center, it can be seen that the coordination of an active Ti changes from a distorted tetrahedral structure in the bare TS-1 to a distorted octahedral conformation in the adsorption complex (Figure 7). The latter involves three Ti-O-Si bridging oxygens, titanol oxygen, a neighboring silanol oxygen, and one of the two oxygens of H_2O_2. This

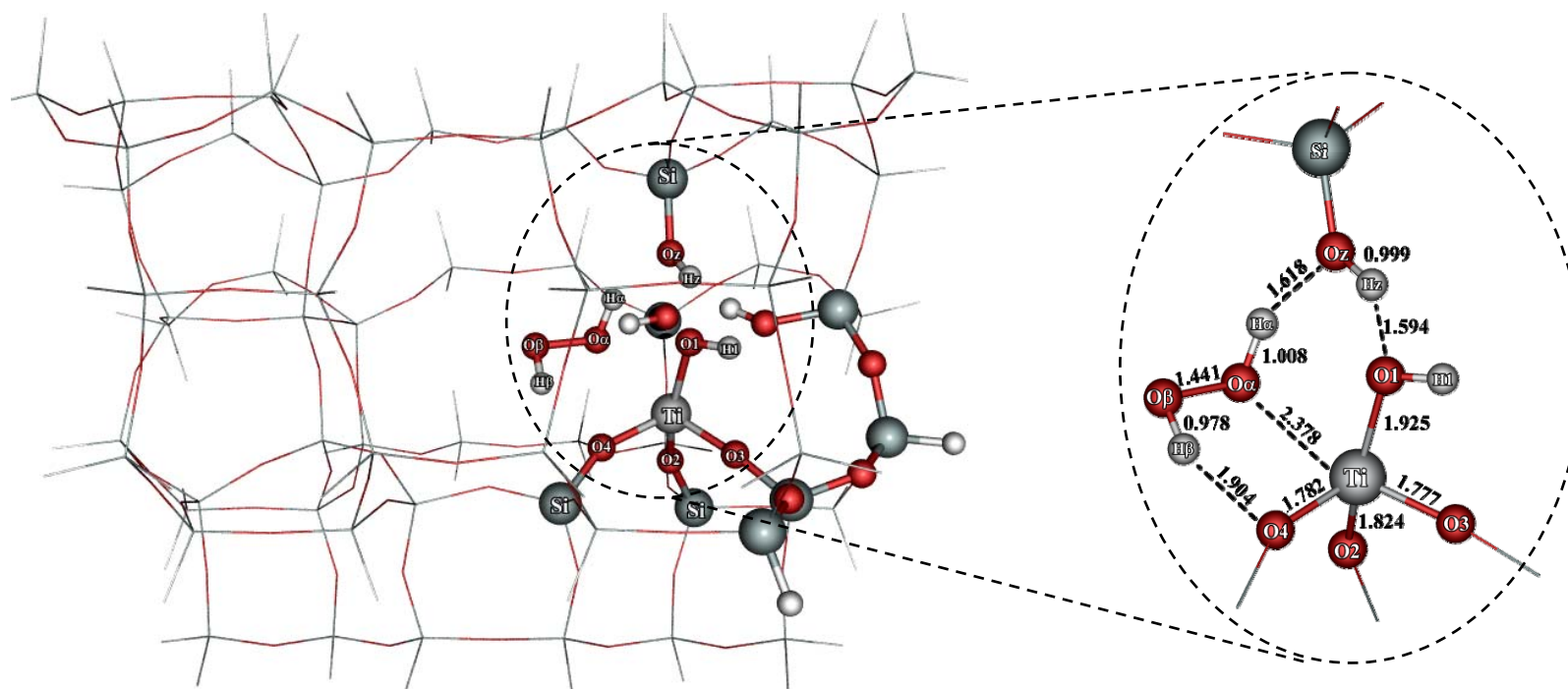configuration can not be obtained when using a nondefect model owing to the restriction of the zeolite framework.

Figure 5 Showing the optimized structures of adsorption complex (**Ads_1**) of TS-1 and H_2O_2 calculated at the 9T/65T ONIOM2(B3LYP/6-31G(d,p):UFF) method.
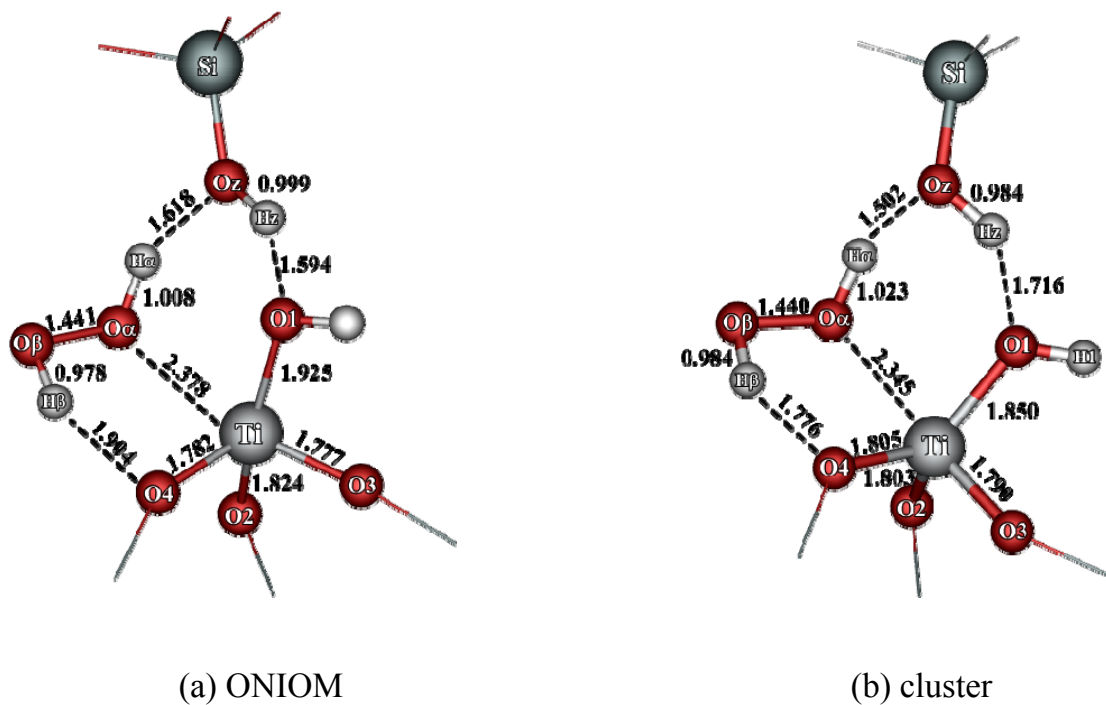
(a) ONIOM   (b) cluster

Figure 6   Showing (a) the optimized structures of adsorption complex (**Ads_1**) of TS-1 and H_2O_2 calculated at the 9T/65T ONIOM2(B3LYP/6-31G(d,p):UFF) method and (b) at the 9T B3LYP/6-31G(d,p) cluster. Some of the quantum region (balls and sticks) and the rest UFF region (lines) are omitted for clarity.
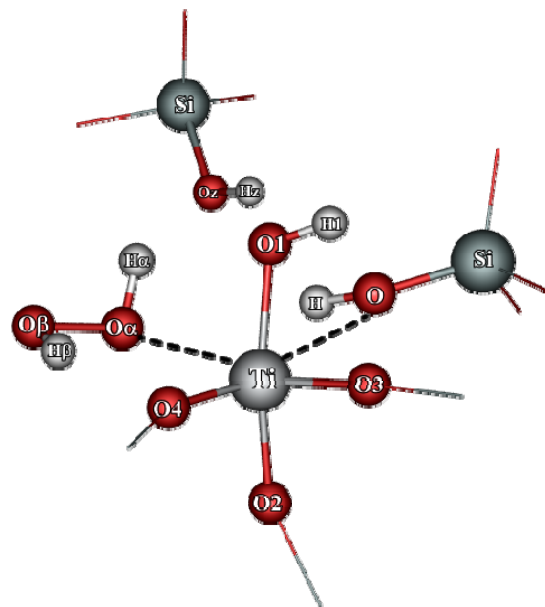
Figure 7 Showing distorted octahedral conformation of adsorption complex (Ads_1) by close-up Figure 5. Some of the quantum region (balls and sticks) and the rest UFF region (lines) are omitted for clarity.

Table 2 Selected optimized geometrical parameters of the adsorption complex (**Ads_1**), transition states (**ts_1** and **ts_2**), and **Int_4** using the 9T B3LYP/6-31G(d,p) cluster and the 9T/65T ONIOM2(B3LYP/6-31G(d,p):UFF) scheme.

	Ads_1		**ts_1** (single H)		**ts_2** (double H)		**Int_4** (Figure 14)	
	cluster	ONIOM	cluster	ONIOM	cluster	ONIOM	cluster	ONIOM
bond distance (Å)								
Ti-O1	**1.850**	1.925	**1.968**	1.977	**1.929**	2.012	**3.764**	3.810
Ti-O2	**1.803**	1.824	**1.806**	1.803	**1.807**	1.812	**1.784**	1.794
Ti-O3	**1.790**	1.777	**1.784**	1.783	**1.804**	1.789	**1.805**	1.799
Ti-O4	**1.805**	1.782	**1.763**	1.742	**1.794**	1.775	**1.748**	1.732
Ti-O$_\alpha$	**2.345**	2.378	**2.290**	2.336	**2.145**	2.224	**1.910**	1.934
Ti-O$_\beta$	**3.296**	3.297	**3.234**	3.289	**3.118**	3.193	**2.308**	2.303
O$_\alpha$-O$_\beta$	**1.440**	1.441	**1.444**	1.443	**1.443**	1.443	**1.460**	1.455
O$_\alpha$-Oz	**2.442**	2.508	**3.069**	2.878	**2.360**	2.368	**2.439**	2.371
O$_\alpha$-H$_\alpha$	**1.023**	1.008	**1.192**	1.186	**1.320**	1.168	**-**	-
O$_\beta$-H$_\beta$	**0.984**	0.978	**0.977**	0.973	**0.980**	0.976	**1.009**	1.005
Oz-O1	**2.570**	2.480	**2.536**	2.514	**2.390**	2.361	**2.799**	2.871
Oz-Hz	**0.984**	0.999	**0.977**	0.982	**1.076**	1.143	**1.007**	1.016
bond angle (°)								
∠O$_\alpha$-H$_\alpha$-Oz	**150.0**	144.6	**101.8**	95.4	**152.6**	156.8	-	-
∠Oz-H1-O1	**142.8**	145.1	**65.1**	65.6	**153.2**	155.2	-	-

The final ONIOM2 adsorption energy is exothermic by 11.6 kcal/mol (Table 3), which is relatively lower than that obtained in the previous theoretical small cluster study at the BPW91 functional of 17 kcal/mol (Wells *et al.*, 2004). Direct comparison with the experimental report might provide quantitative acceptability of the functionals; unfortunately, the adsorption energy of H_2O_2 on TS-1 has never been reported. Recently, the adsorption energies of H_2O and NH_3 vapor on TS-1 have been measured by means of a heat-flow microcalorimeter (Bordiga *et al.*, 2002). It has been found that the adsorption energy of H_2O on the Ti center was approximately exothermic by much less than 15 kcal/mol and not directly detectable from this study, whereas it was observed to be exothermic by about 18 kcal/mol for NH_3, which is a much stronger Lewis base. Based on these experimental evidences, it can be seen that the adsorption energy calculated at the ONIOM2(B3LYP/6-31G(d,p):UFF) seems to be the more reliable value as compared to the small cluster calculation using BPW91 functional, which gives a much overestimated value for this system. Furthermore, using a small quantum cluster with neglect of the zeolite framework constraints may cause unexpectedly high interaction energy. As found in our present study, the small 9T quantum cluster calculation leads to the highly exothermic adsorption energy of 19.4 kcal/mol (Table 3) while it is exothermic only by 11.6 kcal/mol for the 30T quantum cluster embedded in the UFF force field calculation (single point energy of the optimized structure of the 9T/65T ONIOM2 model). Comparing this with the nondefect models in previous theoretical studies where the adsorption energy was exothermic by about 8-9 kcal/mol (Bonino *et al.*, 2004; Vayssilov and Van Santen, 1998), the defect models are found to give higher exothermic adsorption energy (11.6 kcal/mol) due to the relatively high flexibility of the Ti active site that allows it to accommodate lower energy configurations of the adsorption complex and the presence of the neighboring silanol groups resulted

from a Si vacancy that provides the great potential for stabilizing the adsorption complex through the H-bond formation.

2. Oxidative active site formation.

Although the physisorption of H_2O_2 on the Ti active center is theoretically observable (Barker *et al.*, 2001; Munakata *et al.*, 2001; Sever and Root, 2003a; Sinclair and Catlow, 1999), an undissociated adsorption form has never been reported experimentally. Instead, the dissociated adsorption known as the titanium hydroperoxo species, Ti-OOH, is undoubtedly detected after TS-1 is contacted with the H_2O_2/H_2O solution (Bonino *et al.*, 2004; Lin and Frei, 2002). This species is believed to be the active oxidizing intermediate in the Ti/H_2O_2 system. However, an elementary step of the oxidative active site formation has never been focused on intensively. Recently, Wells and coworkers have proposed the Ti-OOH formation through the direct proton transfer from H_2O_2 to the titanol OH group with the calculated activation energy of 15 kcal/mol (Wells *et al.*, 2004). Sever and Root have shown that the Gibbs activation energy for Ti-OOH formation is lowered by 5-6 kcal/mol when a protic solvent molecule is present in the hydrogen-bonded bridging position (Sever and Root, 2003a). When considering the physisorption complex in our present study (Figure 5), it can be seen that the Ti-OOH formation can be accomplished either via a direct single proton transfer or an indirect double proton transfer mechanism. A proton of H_2O_2 is directly attached to the titanol OH group in the one-step single proton transfer mechanism whereas, in the one-step double proton transfer mechanism, it is transferred to the proximal silanol OH group, which serves as a proton donor-acceptor group. All selected optimized structural parameters for the single and double proton transfer transition states are listed in Table 2.

Figure 8 shows the transition state structure of a single proton transfer mechanism. The imaginary vibrational mode obtained from the frequency calculation corresponds to the protonation of the titanol group. The H_α of H_2O_2 is directly migrating to the titanol OH group at the same time that the O_α is coordinating with the Ti active center. The O_α-H_α bond is breaking and lengthened to be 1.186 and 1.192 Å for the ONIOM2 model and 9T cluster, respectively, whereas the Ti···O_α separation is contacted to be 2.336 vs 2.290 Å. This process converts a poor leaving group (OH^-) into a good one (H_2O). Therefore, a water molecule is being developed during the formation of an oxidative active species. With respect to **Ads_1,** the activation energies for the direct proton transfer are estimated to be 10.8 and 11.8 kcal/mol for the ONIOM2 and the 9T cluster, respectively. An alternate transition state structure looks more complicated than a single proton transfer. As shown in Figure 9, the protonation takes place through a double proton transfer mechanism with the assistance of a nearby silanol group. Instead of passing Hα directly to the titanol OH group, the H_2O_2 transfers its H_α to the neighboring silanol OH group, which behaves like a bridge linking between H_2O_2 and a titanol group. The vibrational mode of an imaginary frequency shows the synchronized dual proton transfer mechanism where two protons, one from H_2O_2 and another from silanol OH group, move toward the partial negative-charge oxygen atoms (Oz and O1) simultaneously. In this way, the activation energies are reduced to 2.6 and 4.2 kcal/mol for the ONIOM2 and the 9T cluster, respectively (Table 3). Unlike in the single proton transfer mechanism where one of the two hydrogen bonds in the adsorption complex is necessary to break before the protonation, the pre-hydrogen-bonded system increases the degree of proton transfer in the double proton transfer process. From these results, it can be concluded that, in the defect active site model of TS-1, the formation of an oxidative active species is preferred to occur via the double proton transfer mechanism.
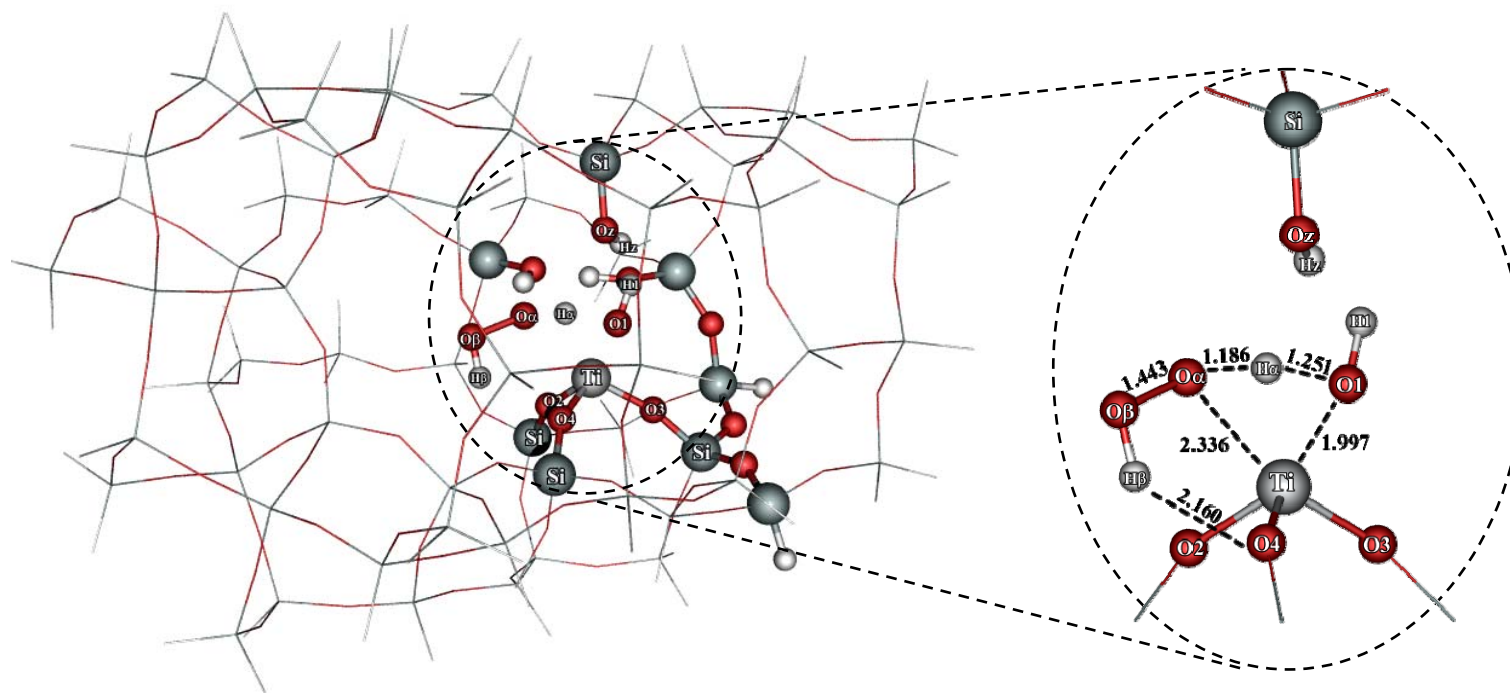
Figure 8 Showing optimized geometrical structures of the single proton mechanisms using the 9T/65T ONIOM2(B3LYP/6-31G(d,p):UFF).
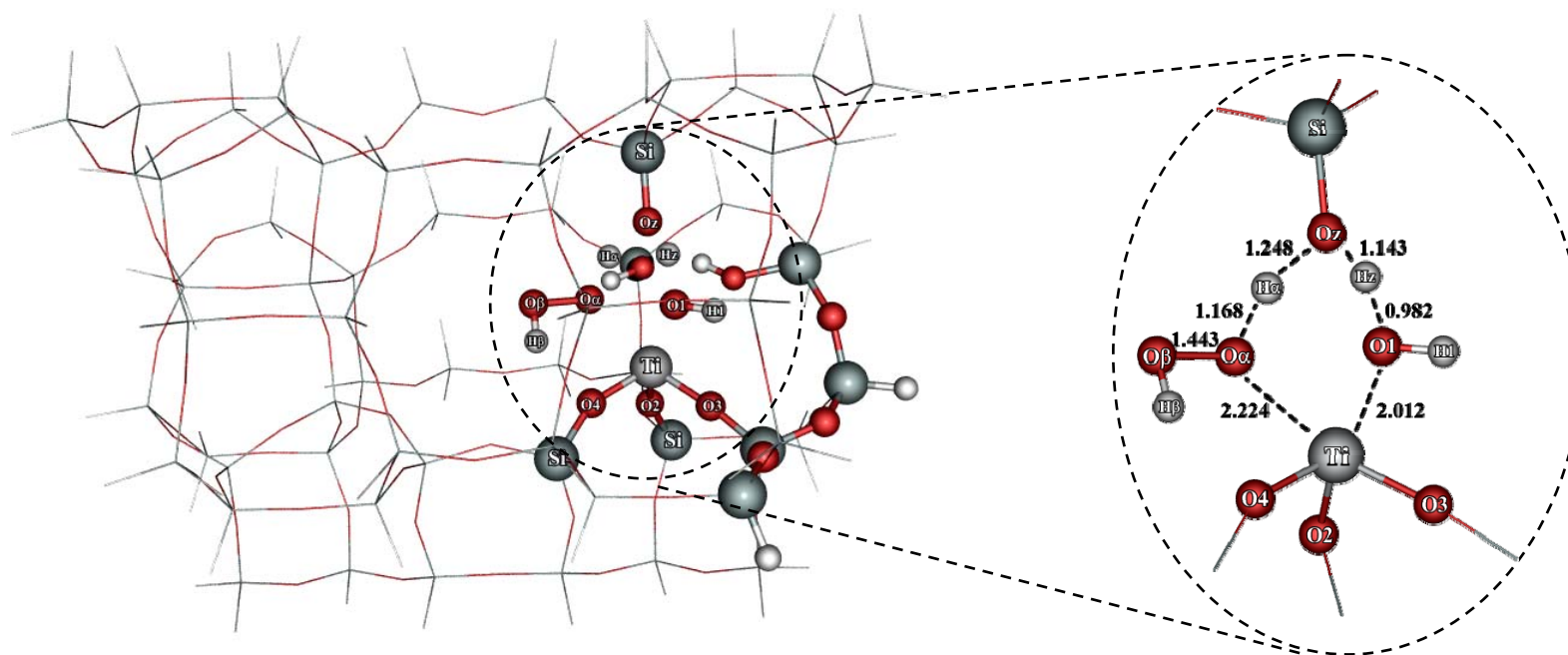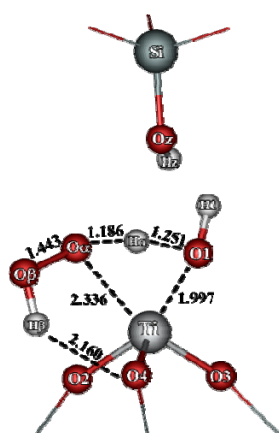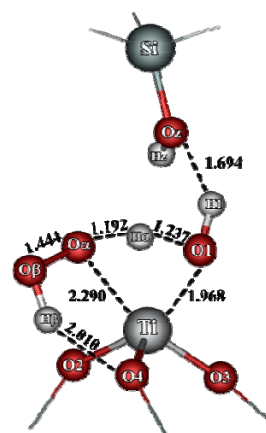
Figure 9 Showing optimized geometrical structures of the double proton mechanisms using the 9T/65T ONIOM2(B3LYP/6-31G(d,p):UFF).
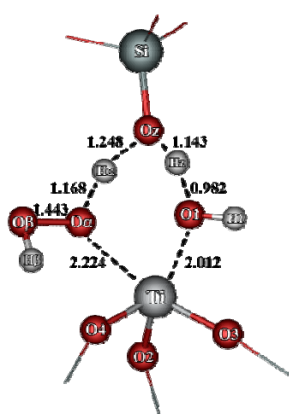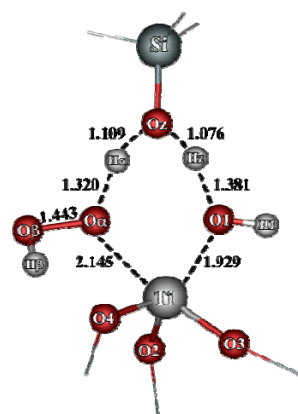
(a) ONIOM   (b) cluster

single proton transfer mechanism (**ts_1**)

(c) ONIOM   (d) cluster

double proton transfer mechanism (**ts_2**)

Figure 10 Optimized geometrical structures of (a) and (b) the single proton transfer and (c) and (d) the double proton transfer mechanisms using the 9T/65T ONIOM2(B3LYP/6-31G(d,p):UFF) scheme (left) and the 9T B3LYP/6-31G(d,p) cluster (right).

3. Stability of the oxidative active species

The proton transfer process is completed with the formation of a water molecule and the titanium hydroperoxo complexes (Ti-OOH). These species have been modeled as the oxidative active species, which can be formed either in a mono (η^1) or bi-dentate (η^2) form. Their relative stability with respect to the adsorption complex (**Ads_1**), however, depends on the environmental surroundings as shown in Figures 11-15. The mono-dentate structure (**Int_1**), the first Ti-OOH species formed after H_2O_2 contacted with the Ti active center, is the most stable configuration of the TS-1 defect model. It is more stable than an undissociated adsorption complex, **Ads_1**, by 10.3 and 7.0 kcal/mol for the ONIOM2 and the 9T cluster models, respectively. Its hydrated form allows the Ti active center to form a likely stable octahedral structure with the coordination number of six (Figure 16), which is larger than those of the bi-dentate structures (**Int_2**, **Int_3**, and **Int_4**) of five. It can be seen that the stability of Ti-OOH species is not only determined by the coordination number of the Ti atom but also by the number of strong hydrogen bonds. For the bi-dentate structures, the **Int_4** is the most stable one when compared to **Int_2** and **Int_3** configurations because its H_β can form a strong hydrogen bond with the water molecule. By using the ONIOM2 model, this conformation is more stable than the physisorbed complex of TS-1/H_2O_2 (**Ads_1**) by 5.3 kcal/mol whereas, when using the 9T cluster model, both **Int_4** and **Ads_1** are equally stable. For the **Int_2** and **Int_3** structures where the acidic hydrogen (H_β) is not directly formed the H-bond with the water molecule, their stability is relatively low when compared to the **Int_4** complex. With respect to the **Ads_1** complex, the **Int_3** configuration is slightly more stable (by 2.3 kcal/mol) when using the ONIOM2 approach but it is somewhat less stable (by about 2.8 kcal/mol) when evaluating with the 9T cluster model. The **Int_2** was found to be the least stable structure. It is less stable than the **Ads_1** complex by 5.4 and 9.7

kcal/mol for the ONIOM2 and 9T cluster models, respectively. All the relative energies with respect to the isolated TS-1 models and H_2O_2 gas and the selected structural parameters of the oxidative active species are listed in Tables 3 and 4, respectively.

Table 3 Relative energies (kcal/mol) with respect to the isolated TS-1 model and H_2O_2 gas of the adsorption complex (**Ads_1**), activation energies of **ts_1** and **ts_2** transition states, and oxidative active species of TS-1 calculated at the 30T/65T ONIOM2(B3LYP/6-31G(d,p):UFF) method and at the 9T B3LYP/6-31G(d,p) cluster approach. The values in parentheses are the activation energies with respect to the **Ads_1** complex.

	cluster	ONIOM
Adsorption complex or **Ads_1** (Figure 5)	-19.4	-11.6
Transition state (activation energy)		
Single proton transfer or **ts_1** (Figure 8)	-7.6 (**11.8**)	-1.8 (**10.8**)
Double proton transfer or **ts_2** (Figure 9)	-15.5 (**4.2**)	-9.0 (**2.6**)
Oxidative active species		
Ti(η^1-OOH) or **Int_1** (Figure 11)	-26.5	-21.9
Ti(η^2-OOH) or **Int_2** (Figure 12)	-9.7	-6.2
Ti(η^2-OOH) or **Int_3** (Figure 13)	-16.7	-13.9
Ti(η^2-OOH) or **Int_4** (Figure 14)	-19.4	-16.9
Ti(η^2-OO-) or **Int_5** (Figure 17)	-	-14.2

Table 4 Selected optimized geometrical parameters of oxidative active species generated along the creation of oxidative active site using the 9T B3LYP/6-31G(d,p) cluster and the 9T/65T ONIOM2(B3LYP/6-31G(d,p):UFF) scheme. Geometries are shown in Figures 11-17.

	Int_1		Int_2		Int_3		Int_4		Int_5	
	cluster	ONIOM	cluster	ONIOM	cluster	ONIOM	cluster	ONIOM	cluster	ONIOM
bond distance (Å)										
Ti-O1	**2.132**	2.168	**4.516**	3.946	**4.195**	4.382	**3.764**	3.810	-	3.440
Ti-O2	**1.789**	1.779	**1.806**	1.788	**1.865**	1.823	**1.784**	1.794	-	1.820
Ti-O3	**1.813**	1.819	**1.787**	1.793	**1.787**	1.799	**1.805**	1.799	-	1.956
Ti-O4	**1.771**	1.756	**1.769**	1.750	**1.742**	1.762	**1.748**	1.732	-	1.728
Ti-O$_\alpha$	**2.000**	2.010	**1.914**	1.954	**1.899**	1.918	**1.910**	1.934	-	1.934
Ti-O$_\beta$	**2.869**	2.915	**2.225**	2.292	**2.077**	2.193	**2.308**	2.303	-	1.944
O$_\alpha$-O$_\beta$	**1.447**	1.446	**1.465**	1.472	**1.472**	1.468	**1.460**	1.455	-	1.456
O$_\beta$-H$_\beta$	**0.977**	0.974	**0.977**	0.975	**1.025**	0.991	**1.009**	1.005	-	-

Titanium peroxo species, Ti-(OO$^-$), in the η^2 configuration is the only one that can be detected experimentally. Its existence has been confirmed by the Raman spectroscopic study of the yellow color of the TS-1/H_2O/H_2O_2 system, which shows the frequency at 618 cm^{-1} (Bonino *et al.*, 2004; Bordiga *et al.*, 2003; Ricchiardi *et al.*, 2001). Although there is no evidence that the Ti-(OO$^-$) is an active speices in the partial oxidation reactions, it can be in equilibrium with the hydroperoxo complexes in the presence of water. The peroxo complex is possibly formed by the evolution of both η^1 and η^2 hydroperoxo species in the presence of water molecule via the formation of H_3O^+/H_2O. Figure 17 shows the Ti peroxo complex, **Int_5**, in bi-dentate manner. Two O atoms of H_2O_2 coordinate to Ti with distances of 1.934 and 1.944 Å. The O-O bond is lengthened from 1.445 Å of an isolated H_2O_2 to 1.456 Å. One of the O atoms forms a hydrogen bond with the next silanol group while the other is stabilized by H_2O and H_3O^+, which form a hydrogen bond to each other. It is to be noted that the peroxo complex could not be formed in the 9T cluster approach and even if, by using the ONIOM scheme but in the absence of an additional water molecule, the result was not altered from the 9T cluster approach. Thus our finding is in accordance with the role of water in hydroperoxo-peroxo interconversion in the TS-1/H_2O/H_2O_2 system (Bonino *et al.*, 2004).

Figure 11 Showing optimized geometrical structures of Ti-hydroperoxo complexes of **Int_1** calculated at the 9T/65T
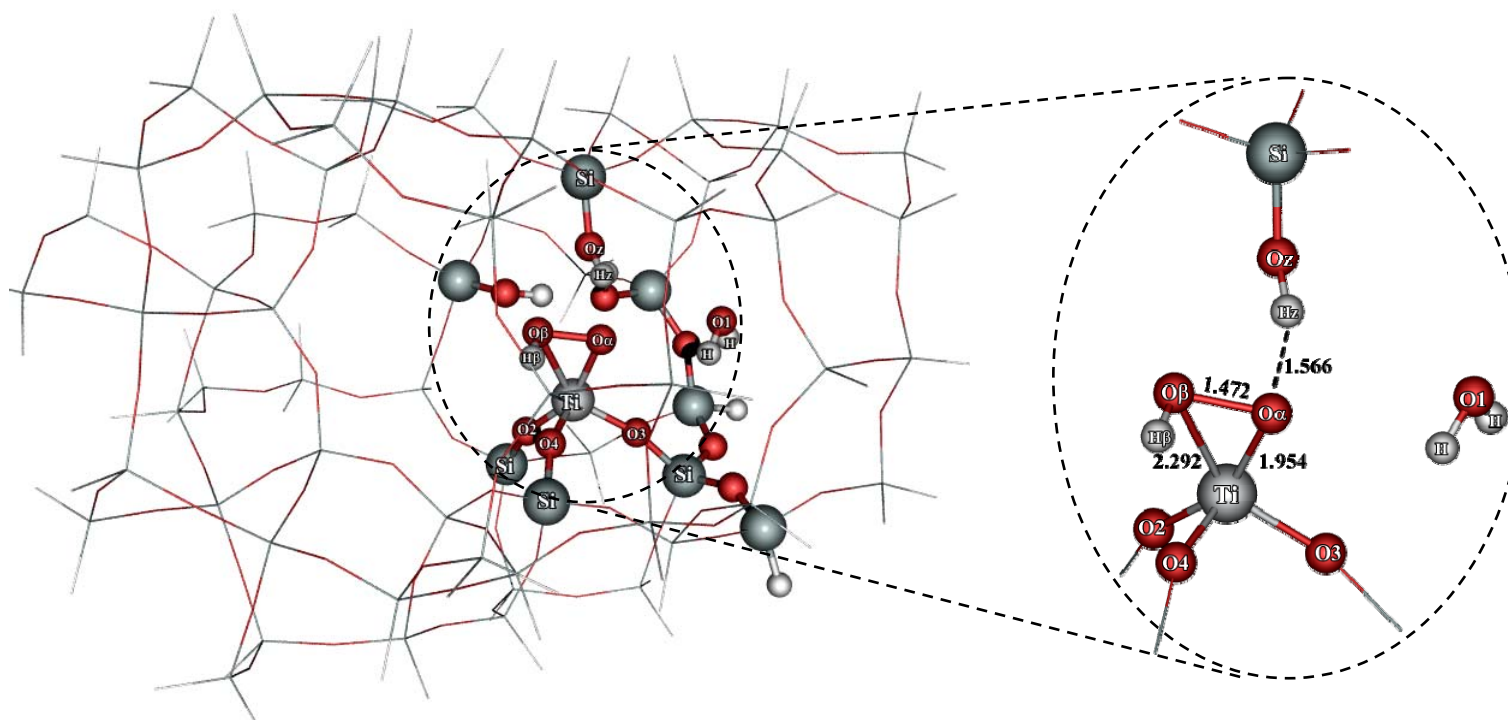ONIOM2(B3LYP/6-31G(d,p):UFF) level of theory

Figure 12 Showing optimized geometrical structures of Ti-hydroperoxo complexes of **Int_2** calculated at the 9T/65T ONIOM2(B3LYP/6-31G(d,p):UFF) level of theory
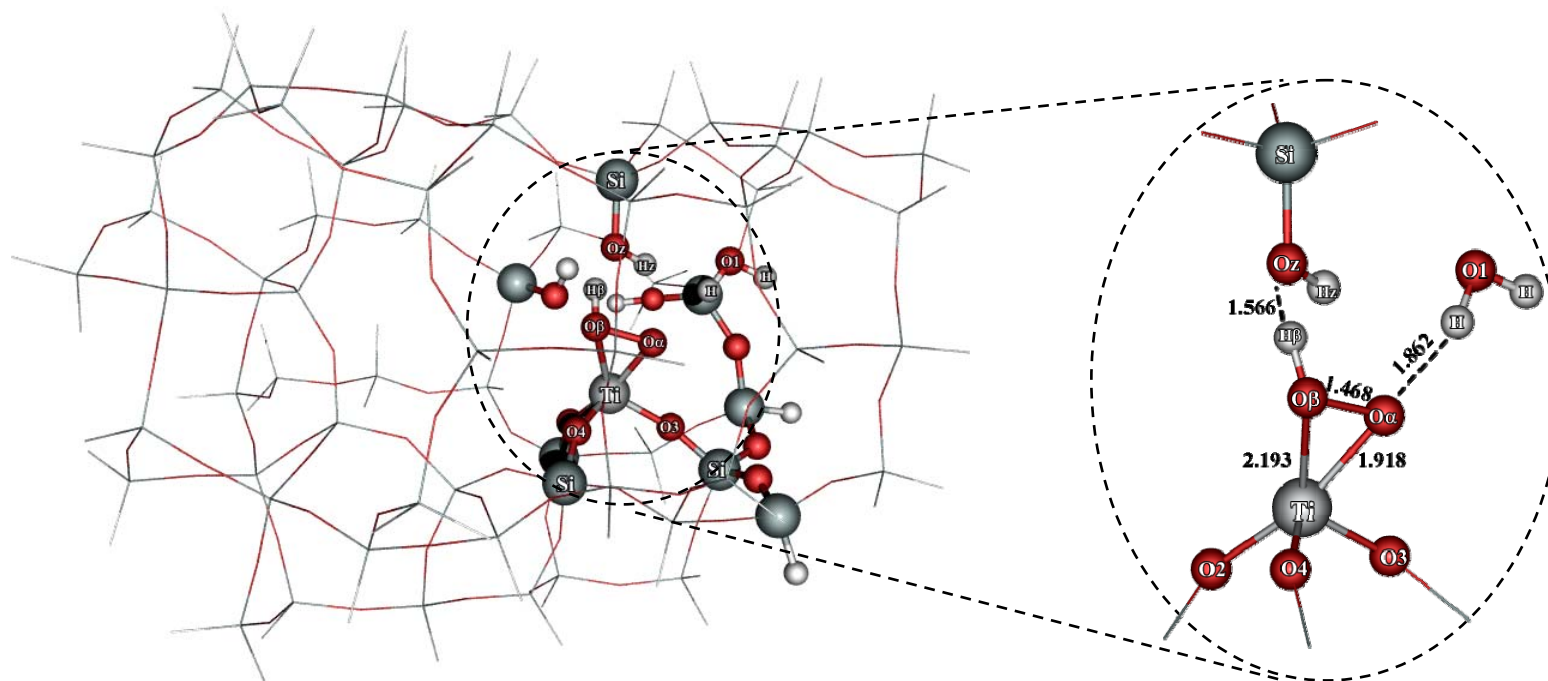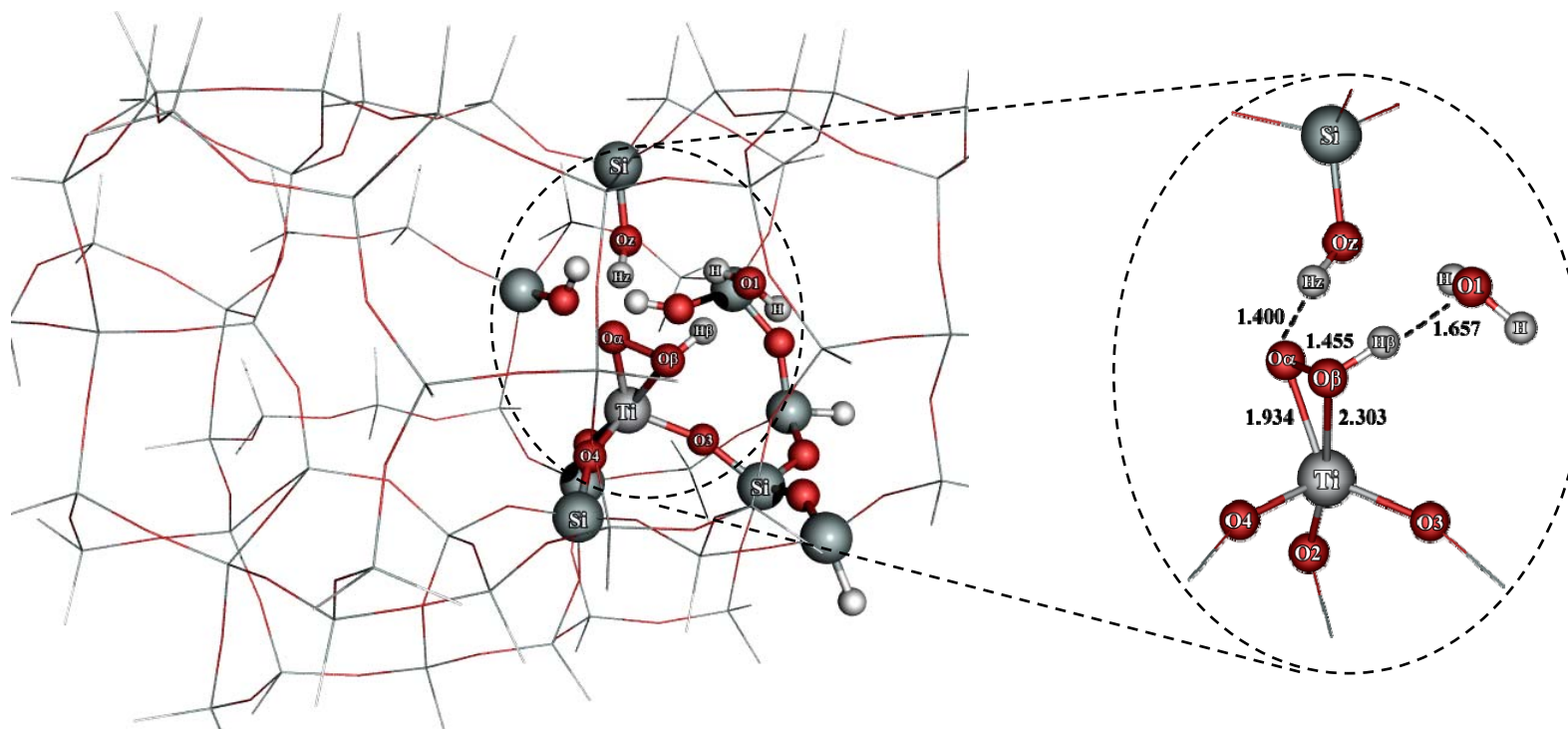
Figure 13 Showing optimized geometrical structures of Ti-hydroperoxo complexes of **Int_3** calculated at the 9T/65T ONIOM2(B3LYP/6-31G(d,p):UFF) level of theory

Figure 14 Showing optimized geometrical structures of Ti-hydroperoxo complexes of **Int_4** calculated at the 9T/65T ONIOM2(B3LYP/6-31G(d,p):UFF) level of theory.
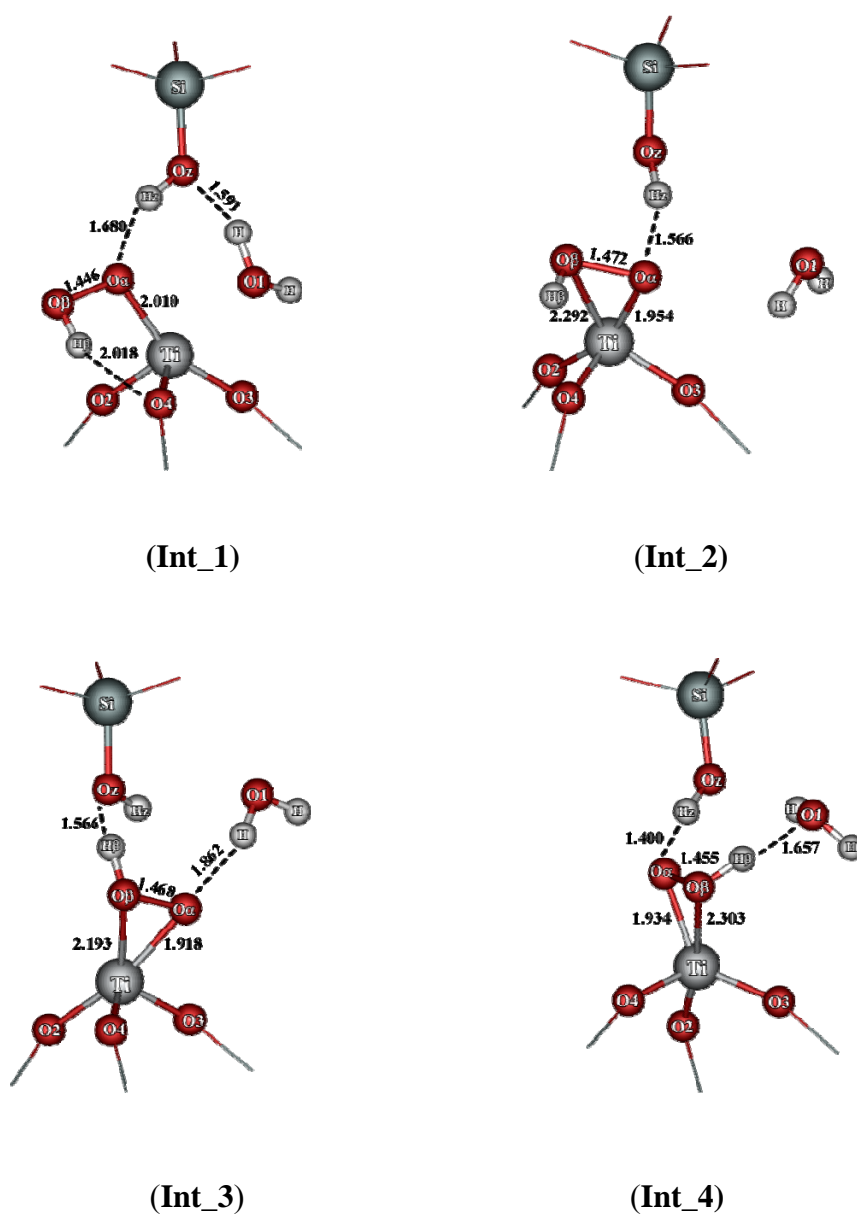
(Int_1) (Int_2)

(Int_3) (Int_4)

Figure 15 Optimized geometrical structures of Ti-hydroperoxo complexes in different conformations calculated at the 9T/65T ONIOM2(B3LYP/6-31G(d,p):UFF) level of theory. The conformations obtained from the 9T B3LYP/6-31G(d,p) cluster calculations are very similar to the ONIOM2 results, and thus are omitted.
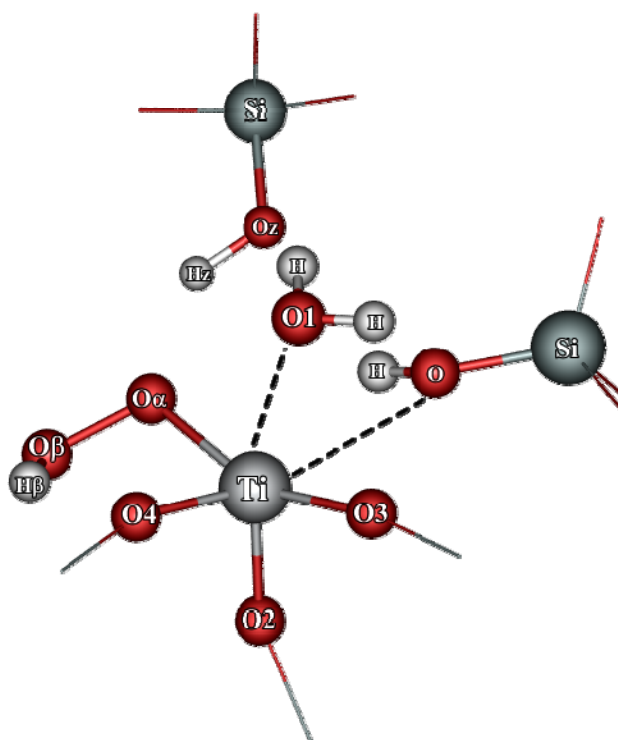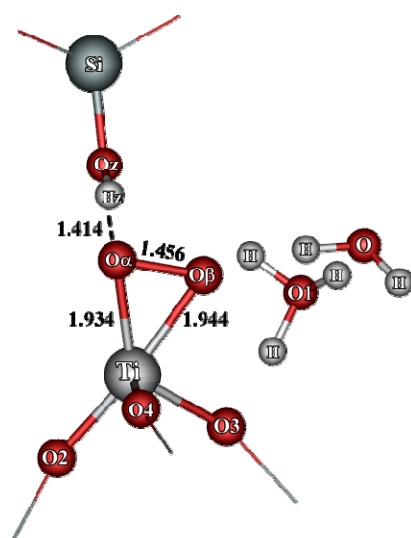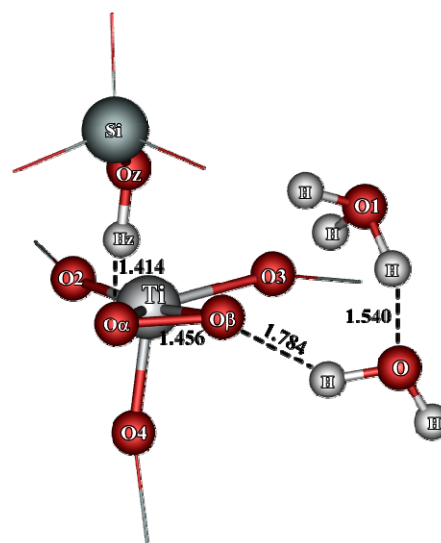
Figure 16 Showing the close-up distorted octahedral conformation of adsorption complex (**Int_1**) in Figure 11. Some of the quantum region (balls and sticks) and the rest UFF region (lines) are omitted for clarity.

Int_5   top view of **Int_5**

Figure 17 Showing optimized geometrical structure of Ti-hydroperoxo complexes of **Int_5** calculated at the 9T/65T ONIOM2(B3LYP/6-31G(d,p):UFF) level of theory.

4. Epoxidation of unsaturated hydrocarbons

Several stable intermediates, including titanium hydroperoxo complexes, Ti-(OOH), in mono- and bi-dentate structures as well as the titanium peroxo complex, Ti-(OO), have been proposed to be active species in the epoxidation of unsaturated hydrocarbons (Feixue *et al.*, 2002; Mimmoun *et al.*, 1982; Yamase *et al.*, 1996). Although the peroxo complex plays a role in the Ti-peroxo and Ti-hydroperoxo interconversion in the aqueous solution (Bonino *et al.*, 2004), it exhibits poor catalytic activity toward partial oxidation reactions. Thus, in this study, we focus only on the Ti-hydroperoxo species as oxidative active sites. Only the bi-dentate structures are considered to be involved in the partial oxidation since the mono-dentate form is too compact to be accessible for the olefins. From our calculations, **Int_3**, and **Int_4** are the most energetic stable configurations of the bi-dentate structures. These two different conformations allow us to investigate the ethylene attack at O_α of hydroperoxo species in the straight channel and cross section of the zeolite pore for **Int_3**, and **Int_4**, respectively. Ignorance of the ethylene attack at O_β mechanism has been elucidated by various previous studies. Tantanak and co-workers have shown that the activation barrier for the ethylene attack at the proximal O_α atom is about 20 kcal/mol, lower than that at the distal O_β atom (Tantanak *et al.*, 1998). Yudanov investigated a distal attack mechanism which involved the concerted cleavage of the O_β-O_α bond and proton transfer from O_β to O_α. The activation barrier was found to exceed the barrier for the proximal attack by about 13 kcal/mol (Yudanov *et al.*, 1999). By using the unconstrained first shell coordination titanium hydroperoxo cluster, including solvent effects, Sever demonstrated that the ethylene attack at the proximal O_α atom reduced the Gibbs free energy changes by 5 kcal/mol (Sever and Root, 2003b). Limtrakul et al. (Limtrakul *et al.*, 2004) and Thomson et al. (Wells *et al.*, 2004) have also proposed the proximal attack for the epoxidation of ethylene and

propylene without solvent, respectively. Therefore, we considered only the ethylene attack at O_α in the oxygen abstraction step.

When the titanium hydroperoxo complex has been formed, it can rapidly interact with ethylene either via the O_α or H_β site, however, we could not locate the stable ethylene adsorbed on O_α of $Ti(\eta^2\text{-OOH})$. This is due to the weak repulsion between O_α and the π bond of ethylene. The ethylene molecule preferred to reside away from the Ti-hydroperoxo oxygenated species. This is in agreement with previous theoretical studies using small cluster models where ethylene prefers to interact with $Ti(\eta^2\text{-OOH})$ by forming the hydrogen bond with the $O_\beta\text{-}H_\beta$ moiety with adsorption energies of 0.9-2.6 kcal/mol (Bonino *et al.*, 2004). Nevertheless, we have not proposed this adsorption complex in our pathway because their conformations do not allow for the oxygen abstraction. Furthermore, to overcome this process, some energy must be added to break the hydrogen bond between ethylene and the $O_\beta\text{-}H_\beta$ group.

As mentioned previously, there are two regions where the epoxidation takes place: at the cross section and the straight channel of the zeolite pore. Figures 18-19 show two locations of transition state complexes of the ethylene epoxidation. It is found that the epoxidation of ethylene at the straight channel requires much higher energy (6.0 and 6.6 kcal/mol for the ONIOM2 and the 9T cluster, respectively) to overcome the activation barrier (E_a) as compared to at the cross section. This is attributed to the zeolite framework constraint of the straight channel which becomes constricted when ethylene is introduced. The activation barrier in the straight channel is certainly expected to be larger when long chain or bulky olefin molecules are considered. Thus, in this study, only the cross section regions are anticipated to accommodate all bulky transition state complexes in the epoxidation pathway. The single point 30T/65T ONIOM2(B3LYP/6-31G(d,p):UFF) apparent activation energy, which is the

energy difference between the transition state and the isolated reactants, for the ethylene epoxidation is calculated to be 15.5 kcal/mol. This value is in agreement with the work of Limtrakul and co-workers for the ethylene epoxidation (15.3 kcal/mol) on the small quantum cluster embedded in the Madelung potential of the zeolite framework (Limtrakul *et al.*, 2004). Sever and Root reported the activation barrier of the ethylene epoxidation by using the first shell unconstrained Ti(η^2-OOH) cluster with one water ligand to be 14.5 kcal/mol (Sever and Root, 2003b). Although we are not able to acquire experimental data on the ethylene epoxidation, our apparent activation energy is very encouraging when compared to the related work of Langhendries and co-workers (Langhendries *et al.*, 1999). They published the apparent activation energy of 15.5±1.5 kcal/mol for the epoxidation of 1-hexene in the TS-1/CH_3OH/H_2O_2 system. However, when the zeolite framework effect was not taken into account, the apparent barrier (E_{app}) was disappeared. This usually happens since the local active site represented only by a small cluster model neglects all the steric hindrances which may encounter when dealing with the bulky transition state complexes. The transition state complex of the ethylene epoxidation (**ts_EO1**) involves the proximal Oα abstraction of the ethylene π bond and the O$_\alpha$-O$_\beta$ bond dissociation (Figure 18). With respect to the **Int_4**, the Ti-O$_\alpha$ bond is lengthened from 1.934 to 1.998 Å and from 1.910 to 1.982 Å for the ONIOM2 and the 9T cluster, respectively, whereas the Ti-O$_\beta$ bond is shortened from 2.303 to 2.041 Å (vs from 2.308 to 1.977 Å). These results correspond to the O$_\alpha$-O$_\beta$ bond elongation (from 1.455 to 1.795 Å vs from 1.460 to 1.795 Å). An approach of ethylene to the O$_\alpha$ results in the C=C bond lengthening (from 1.33 to 1.359 vs 1.357 Å). The C-O distance is split into 2.260 and 1.992 Å (vs 2.154 and 2.129 Å), suggesting that the epoxide formation is an asynchronous type mechanism. All selected optimized structures of ethylene epoxidation transition states are documented in Table 5. The overall ethylene oxidation pathway calculated at the 30T/65T

ONIOM2(B3LYP/6-31G(d,p):UFF) method is shown in Figure 20. The same trend is also obtained from the 9T B3LYP/6-31G(d,p) cluster calculation. From the energy profile of the ethylene epoxidation, it can be seen that the O abstraction step is the overall rate determination step (E_a = 32.5 kcal/mol).

Table 5   Selected optimized geometrical parameters of the oxidative active species (**Int_4**), ethylene epoxidation transition states (**ts_EO**), and adsorption complex of TS-1/ethylene oxide (**Ads_EO**) using the 9T B3LYP/6-31G(d,p) cluster and the 9T/65T ONIOM2(B3LYP/6-31G(d,p):UFF) scheme. Energies are the single point calculations of the optimized 9T/65T ONIOM2(B3LYP/6-31G(d,p):UFF) structures using the 30T/65T ONIOM2 scheme. E_{app} is the apparent energies with respect to the isolated reactants and E_a is activation energy with respect to the **Int_4** complex.

|	Int_4		ts_EO		Ads_EO	
	cluster	ONIOM	cluster	ONIOM	cluster	ONIOM
bond distance (Å)						
Ti-O1	**3.764**	3.810	**4.076**	3.872	**3.975**	3.948
Ti-O$_\alpha$	**1.910**	1.934	**1.982**	1.998	**2.382**	2.451
Ti-O$_\beta$	**2.308**	2.303	**1.977**	2.041	**1.832**	1.884
O$_\alpha$-O$_\beta$	**1.460**	1.455	**1.777**	1.795	**2.816**	2.807
O$_\beta$-H$_\beta$	**1.009**	1.005	**0.998**	0.987	**0.991**	0.987
Oz-O$_\beta$	**-**	**-**	**2.881**	2.478	**2.558**	2.460
Oz-Hz	**-**	**-**	**0.974**	0.992	**0.992**	1.021
∠Oz-Hz-O$_\beta$	**-**	**-**	**152.0**	158.4	**155.6**	164.1
C1-C2	**-**	**-**	**1.357**	1.359	**1.469**	1.470
C1-O$_\alpha$	**-**	**-**	**2.154**	2.260	**1.441**	1.439
C2-O$_\alpha$	**-**	**-**	**2.129**	1.992	**1.441**	1.438
energy (kcal/mol)						
E_{app}	**-19.4**	-16.9	**-1.7**	15.5	**-57.9**	-44.8
E_a	**-**	**-**	**17.7**	32.5	-	-
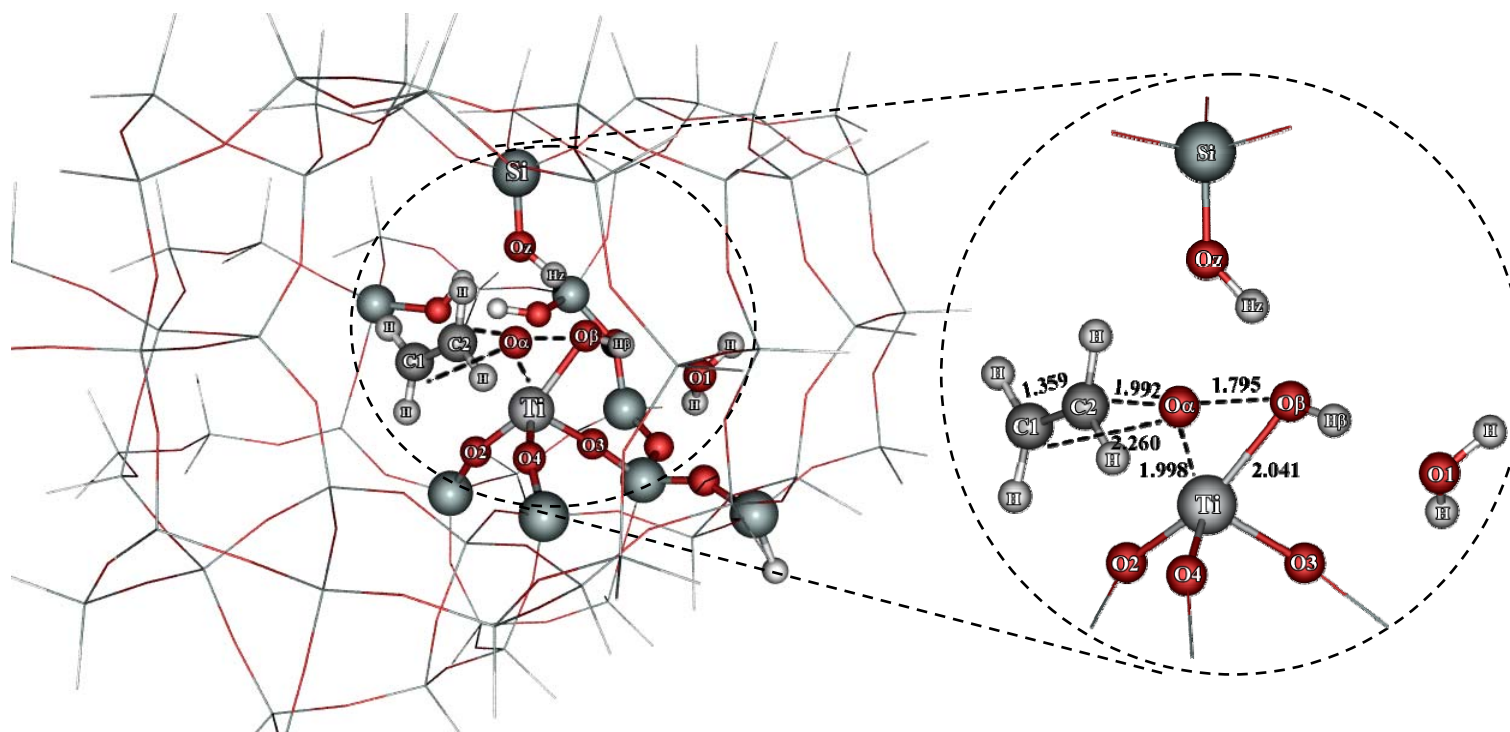
Figure 18 Showing optimized transition state structures of the ethylene epoxidation located at the cross section channel calculated at the ONIOM2(B3LYP/6-31G(d,p):UFF) level of theory.
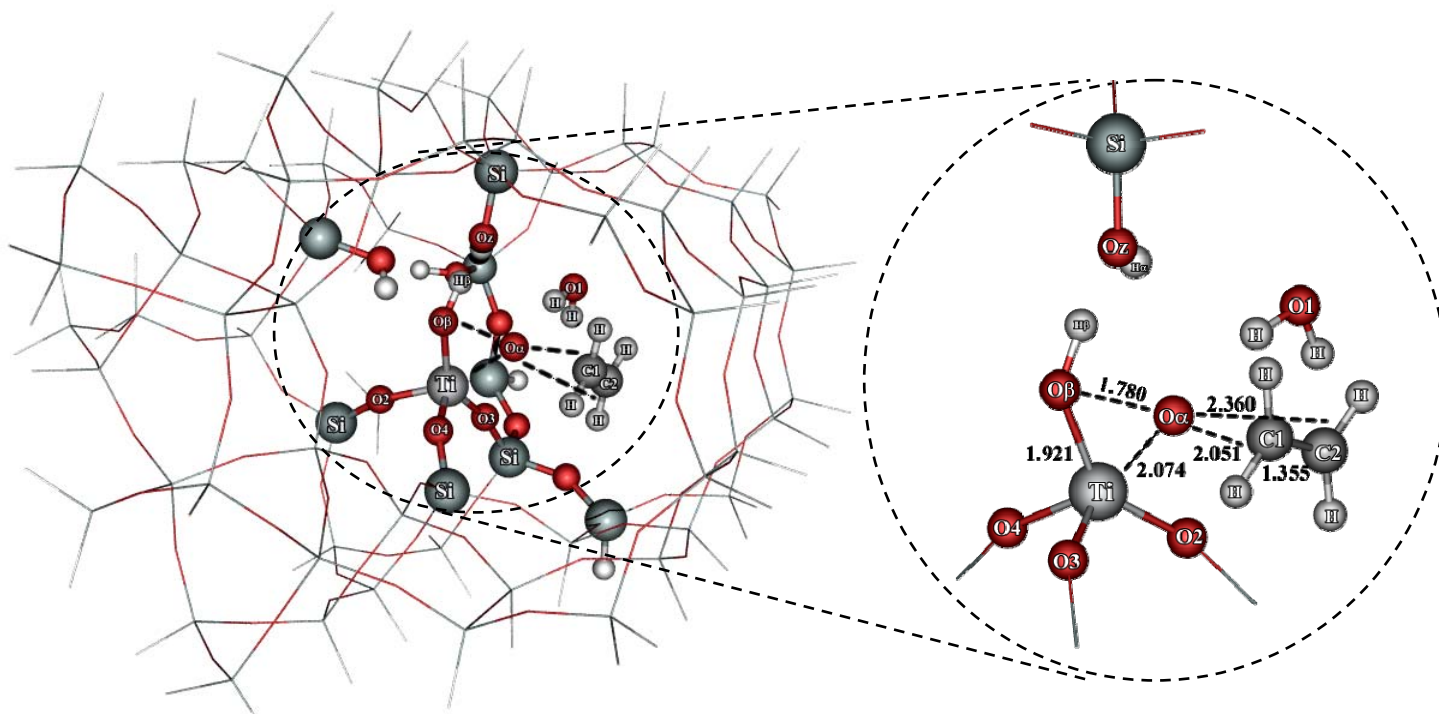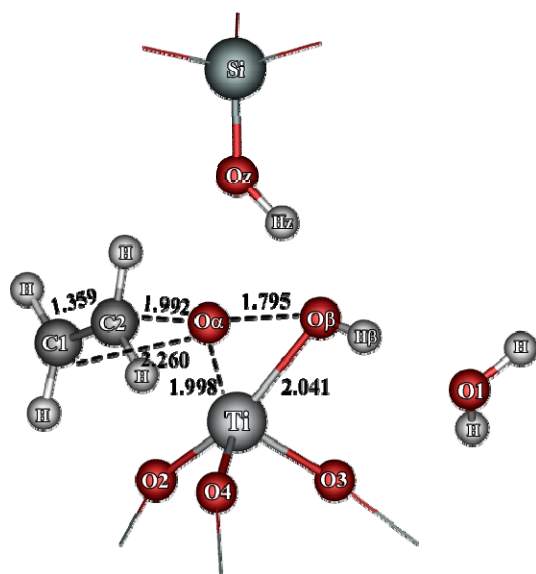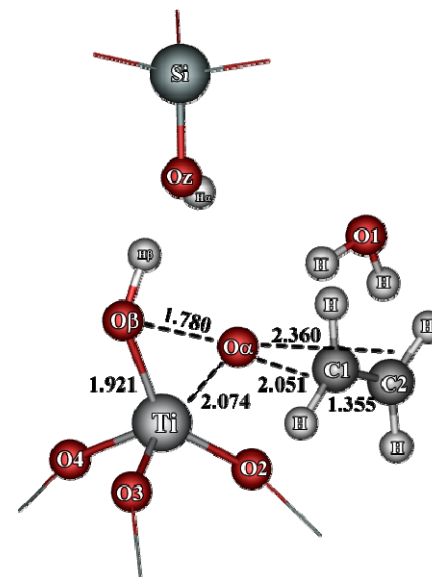
Figure 19 Showing optimized transition state structures of the ethylene epoxidation located at the straight channel calculated at the ONIOM2(B3LYP/6-31G(d,p):UFF) level of theory.

(a) ONIOM (the cross section channel) (b) ONIOM (the straight channel)

Figure 20 Comparision of optimized transition state structures of the ethylene epoxidation located at (a) the cross section and (b) the straight channel. All optimized parameters are obtained from the energy minimization at the ONIOM2(B3LYP/6-31G(d,p):UFF) level of theory. Some parts of the quantum region (balls and sticks) and of MM region (lines) are omitted for clarity. The conformations obtained from the 9T B3LYP/6-31G(d,p) cluster are similar to the ONIOM2 results, and thus are omitted.
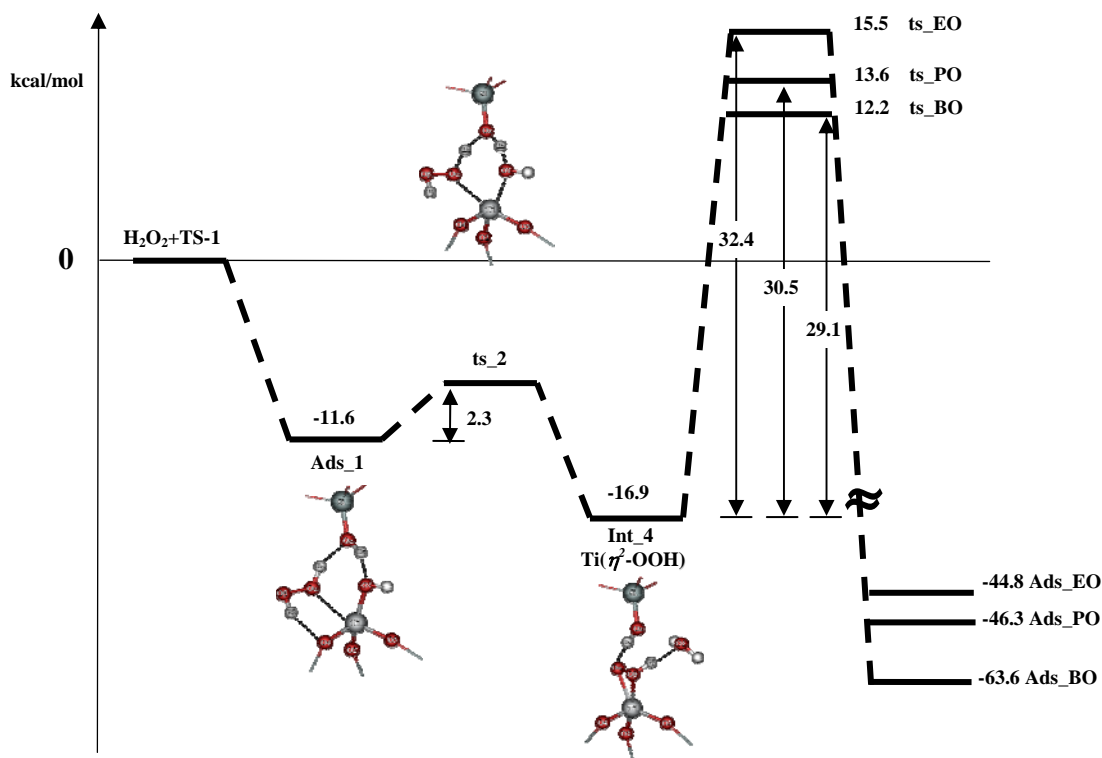
Figure 21 Schematic energy profile of the overall epoxidation reaction of
ethylene, propylene, and trans-2-butylene with H_2O_2 over TS-1
calculated at the ONIOM2(B3LYP/6-31G(d,p):UFF) using the
30T/65T ONIOM cluster scheme.

Further investigation has been performed to determine the effect of the
hydrocarbon chain length on the oxidative reactivity of TS-1 using propylene
and *trans*-2-butylene. The transition state structures of propylene and *trans*-2-
butylene shown in Figure 22-24 and documented in Tables 6-7 are similar to
that of ethylene. Both involve the olefin attack at the proximal O_α of the Ti(η^2-
OOH) complex. Even though the geometrical structures look comparable to the
ethylene epoxidation, the apparent activation barriers are significantly different.
The 30T/65T ONIOM2(B3LYP/6-31G(d,p):UFF) apparent activation energies
are estimated to be 13.6 and 12.2 kcal/mol for propylene and *trans*-2-butylene,
respectively, less than that of ethylene. It should be noted that the activation
barrier decreases with increasing the chain length and number of methyl

groups. This trend is consistent with the 9T B3LYP/6-31G(d,p) cluster and gas phase calculations (Figure 25) of the ethylene, propylene and *trans*-2-butylene epoxidation with H_2O_2 at the same level of theory. Since the substitution of the methyl group, which is a weak electron-donating group, to the active C=C bond leads to the increase of the nucleophilicity of olefinic hydrocarbons, therefore, the reactivity series for the O abstraction is in the order ethylene < propylene < *trans*-2-butylene with the apparent activation energies of 36.3, 34.3, and 32.8 kcal/mol, respectively. The 9T B3LYP/6-31G(d,p) reaction energies are exothermic by 57.9, 59.3, and 59.9 kcal/mol for ethylene, propylene, and *trans*-2-butylene, respectively, which slightly increases with increasing the number of substituted methyl groups, whereas the 30T/65T ONIOM2(B3LYP/6-31G(d,p):UFF) reaction energies of the epoxide formation (Figure 9) are exothermic by 44.8, 46.3, and 63.6 kcal/mol for ethylene, propylene, and *trans*-2-butylene, respectively. The much difference of the reaction energies between propylene oxide and *trans*-2-butylene oxide obtained from the ONIOM2 model is attributed to the van der Waals interactions between epoxide molecules and the zeolite wall, which are sensitive to the size of the adsorbing molecules.
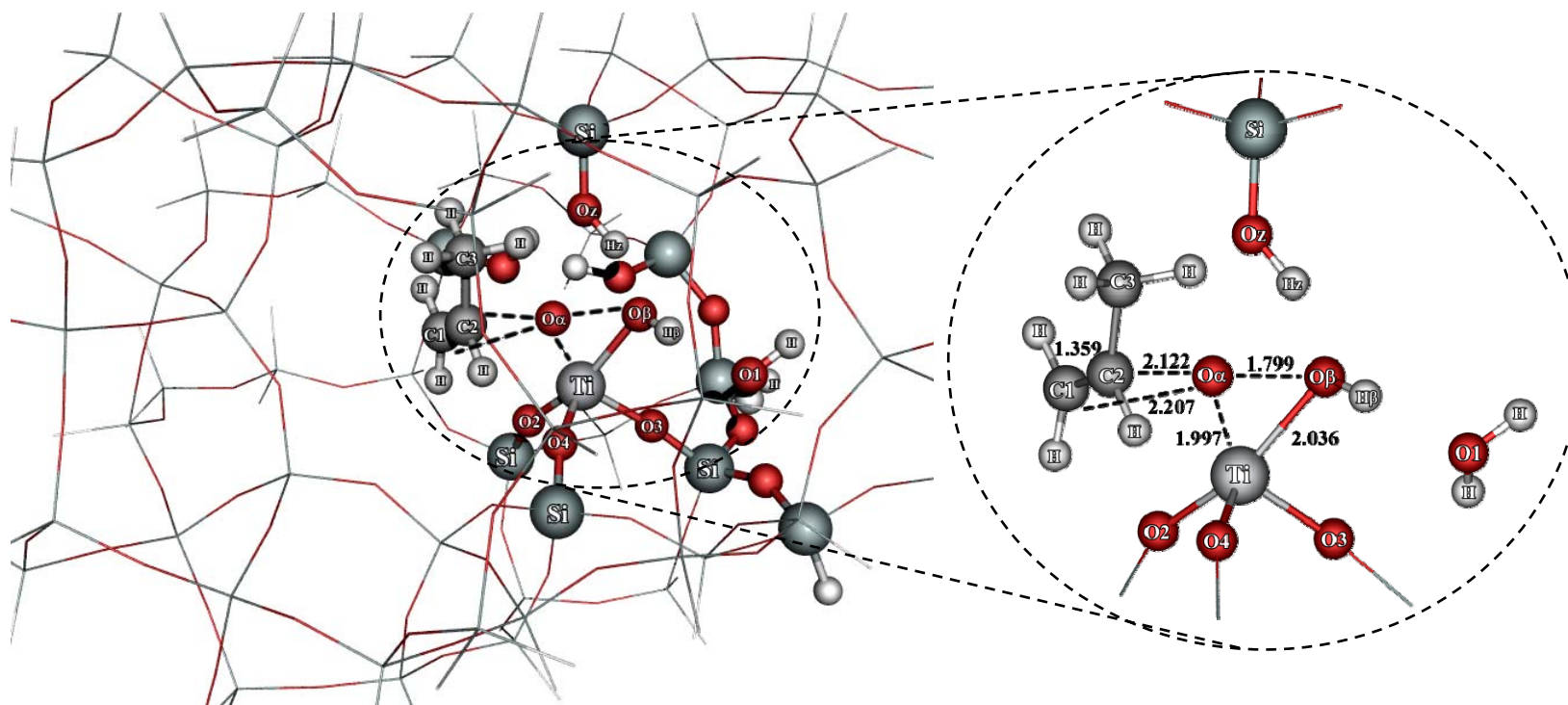
Figure 22 Showing optimized transition state structures of the propylene epoxidation located at the cross section channel calculated at the ONIOM2(B3LYP/6-31G(d,p):UFF) level of theory.
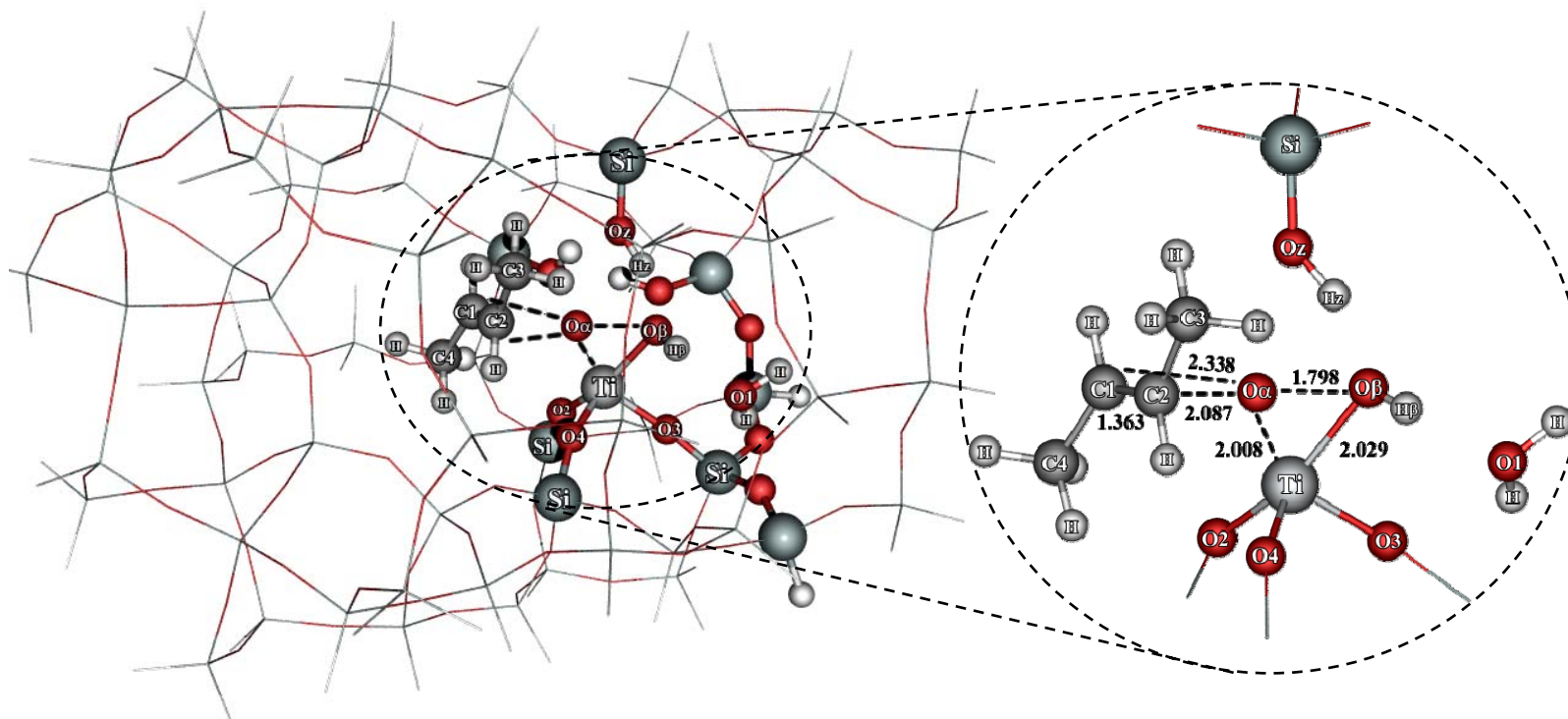
Figure 23 Showing optimized transition state structures of the *trans*-2-butylene epoxidation located at the cross section channel calculated at the ONIOM2(B3LYP/6-31G(d,p):UFF) level of theory.
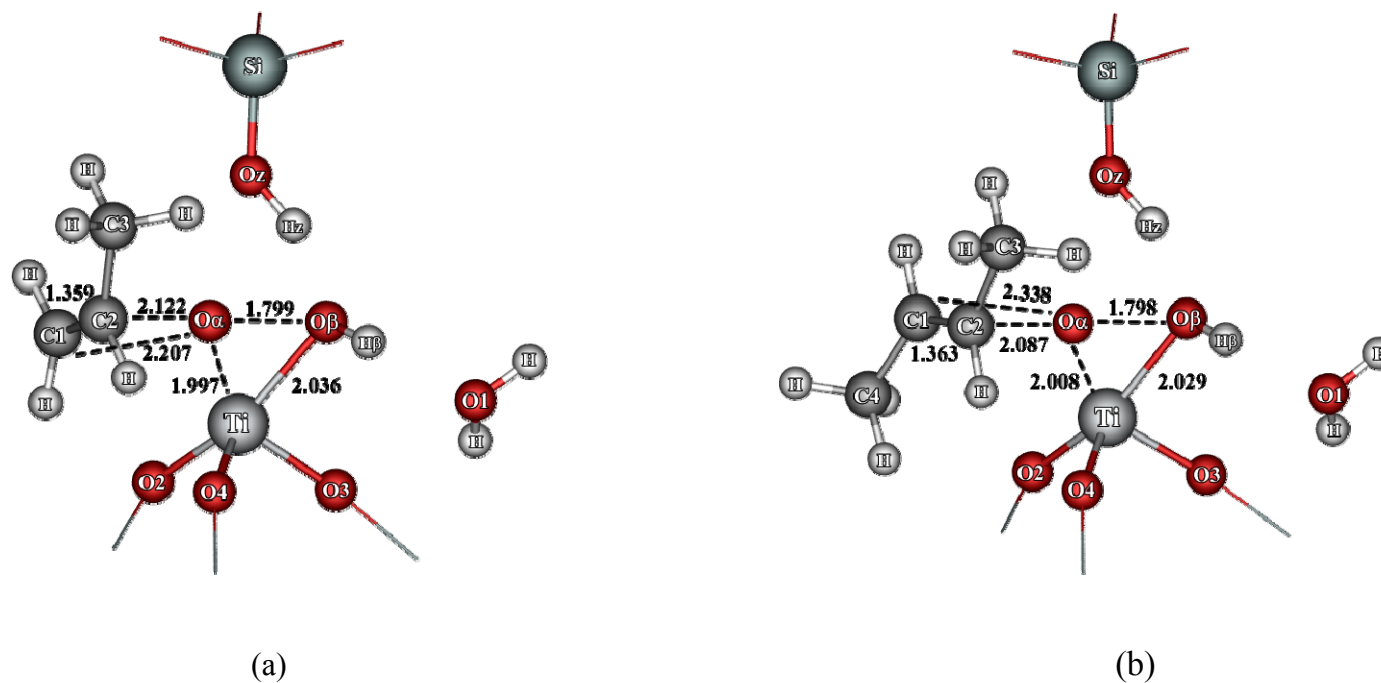
Figure 24 Comparision of optimized transition state complexes of (a) propylene, **ts_PO**, and (b) *trans*-2-butylene, **ts-BO**, epoxidation with H_2O_2 over TS-1 calculated at the 9T/65T ONIOM2(B3LYP/6-31G(d,p):UFF) method level of theory. The conformations obtained from the 9T B3LYP/6-31G(d,p) cluster are similar to the ONIOM2 results, and thus are omitted.

Table 6 Selected optimized geometrical parameters of the oxidative active species (**Int_4**), propylene epoxidation transition states (**ts_PO**), and adsorption complexes of TS-1/propylene oxide (**Ads_PO**) using the 9T B3LYP/6-31G(d,p) cluster and the 9T/65T ONIOM2(B3LYP/6-31G(d,p):UFF) scheme. Energies are the single point calculations of the optimized 9T/65T ONIOM2(B3LYP/6-31G(d,p):UFF) structures using the 30T/65T ONIOM2 scheme. E_{app} is the apparent energies with respect to the isolated reactants and E_a is activation energy with respect to the **Int_4** complex.

	Int_4		ts_PO		Ads_PO	
	cluster	ONIOM	cluster	ONIOM	cluster	ONIOM
bond distance (Å)						
Ti-O1	**3.764**	3.810	**3.907**	3.860	**3.958**	3.930
Ti-O_α	**1.910**	1.934	**1.984**	1.997	**2.409**	2.529
Ti-O_β	**2.308**	2.303	**2.027**	2.036	**1.872**	1.879
O_α-O_β	**1.460**	1.455	**1.776**	1.799	**2.798**	2.977
O_β-H_β	**1.009**	1.005	**0.993**	0.986	**0.990**	0.988
Oz-O_β	-	-	**2.529**	2.468	**2.461**	2.454
Oz-Hz	-	-	**0.992**	0.993	**1.023**	1.020
∠Oz-Hz-O_β	-	-	**162.0**	158.7	**164.7**	164.0
C1-C2	-	-	**1.359**	1.359	**1.470**	1.470
C1-O_α	-	-	**2.177**	2.207	**1.443**	1.442
C2-O_α	-	-	**2.149**	2.122	**1.449**	1.446
energy (kcal/mol)						
E_{app}	**-19.4**	-16.9	**-3.1**	13.6	**-59.3**	-46.3
E_a	-	-	**16.3**	30.5	-	-

Table 7 Selected optimized geometrical parameters of the oxidative active species (**Int_4**), trans-2-butylene epoxidation transition states (**ts_BO**), and adsorption complexes of TS-1/trans-2-butylene oxide (**Ads_BO**) using the 9T B3LYP/6-31G(d,p) cluster and the 9T/65T ONIOM2(B3LYP/6-31G(d,p):UFF) scheme. Energies are the single point calculations of the optimized 9T/65T ONIOM2(B3LYP/6-31G(d,p):UFF) structures using the 30T/65T ONIOM2 scheme. E_{app} is the apparent energies with respect to the isolated reactants and E_a is activation energy with respect to the **Int_4** complex.

	Int_4		ts_BO		Ads_BO	
	cluster	ONIOM	cluster	ONIOM	cluster	ONIOM
bond distance (Å)						
Ti-O1	**3.764**	3.810	**3.887**	3.845	**3.961**	3.921
Ti-O$_\alpha$	**1.910**	1.934	**1.978**	2.001	**2.439**	2.791
Ti-O$_\beta$	**2.308**	2.303	**2.025**	2.029	**1.872**	1.881
O$_\alpha$-O$_\beta$	**1.460**	1.455	**1.776**	1.798	**2.772**	3.162
O$_\beta$-H$_\beta$	**1.009**	1.005	**0.992**	0.987	**0.989**	0.988
Oz-O$_\beta$	-	-	**2.523**	2.476	**2.461**	2.432
Oz-Hz	-	-	**0.993**	0.992	**1.024**	1.023
∠Oz-Hz-O$_\beta$	-	-	**162.1**	158.9	**164.9**	164.2
C1-C2	-	-	**1.363**	1.363	**1.474**	1.472
C1-O$_\alpha$	-	-	**2.310**	2.338	**1.449**	1.446
C2-O$_\alpha$	-	-	**2.115**	2.087	**1.447**	1.442
energy (kcal/mol)						
E_{app}	**-19.4**	-16.9	**-2.9**	12.1	**-59.9**	-63.6
E_a	-	-	**16.4**	29.1	-	-
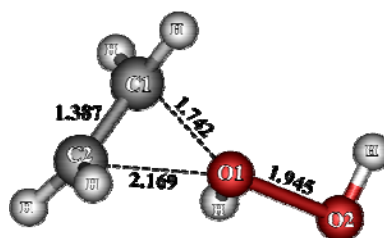
(a)
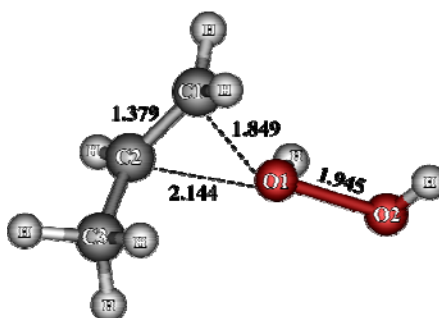
(b)
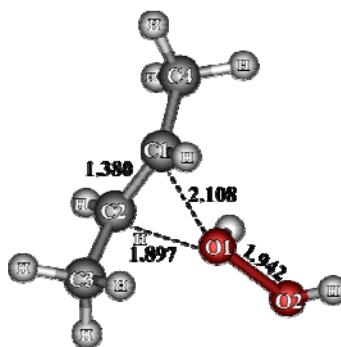
(c)

Figure 25 Optimized gas phase transition state complexes of (a) ethylene (b) propylene, and (c) *trans*-2-butylene epoxidation with H_2O_2 calculated at the B3LYP/6-31G(d,p) level of theory.

CONCLUSION

The partial oxidation of unsaturated hydrocarbons with H_2O_2 over the defect active site of TS-1 catalyst has been systematically studied by using the 9T B3LYP/6-31G(d,p) cluster and the two-layered ONIOM(B3LYP/6-31G(d,p):UFF) methods. In the ONIOM2 model, the energy minimization of initial structures was carried out by using the 9T/65T ONIOM cluster scheme. The single point energies of the minimized structures evaluated at the same level of theory using the 30T/65 ONIOM cluster scheme were reported. The same trend has been obtained from both the 9T cluster and the ONIOM2 calculations. First, a hydrogen peroxide molecule was adsorbed on the Ti atom (**Ads_1**) via the H-bond formation with a neighboring silanol group and a coordinative interaction with the Ti atom. Then, the oxidation pathway of alkenes was proceeded through (i) the formation of an oxidative active site on the Ti atom of TS-1 and (ii) the alkene oxidation. The former was associated with a proton transfer from the hydrogen peroxide to the OH group of the Ti active center to simultaneously develop a water molecule and titanium hydroperoxo intermediates. Two possible mechanisms of this step were investigated, e.g., a direct proton transfer and a double proton transfer with the assistance of the neighboring silanol group. It was found that the double proton transfer mechanism (**ts_2**) was preferred over the direct proton transfer (**ts_1**). The corrected ONIOM2 activation energies for double and direct proton transfer were calculated to be 2.6 and 10.8 kcal/mol, respectively (4.2 and 11.8 kcal/mol, respectively, for the 9T cluster). The titanium hydroperoxo intermediate (**Int_4**) in bi-dentate manner, Ti(η^2-OOH), was selected as the active species in the alkene oxidation process and served as an oxygen atom donor. This species was converted to the titanium peroxo (**Int_5**), Ti(η^2-OO$^-$), complex when an additional molecule was added. In the later step, alkene molecules were introduced to the active site to be oxidized to the epoxide

product. The results showed that the oxygen abstraction step was the rate determining step of the alkene oxidation reaction. The energy barrier of this step was found to decrease with increasing the hydrocarbon chain length and the number of methyl groups. Therefore the nucleophilicity of the alkene molecule was the considerable effect that it had on the activation energy of the oxidation reaction. The 30T/65T ONIOM2(B3LYP/6-31(d,p):UFF) apparent activation energies for ethylene, propylene, and *trans*-2-butylene were predicted to be 15.5, 13.6, and 12.2 kcal/mol, respectively, in good agreement with the experimental epoxidation of 1-hexene in TS-1/CH_3OH/H_2O_2 system of 15.5±1.5 kcal/mol. From these results, it can be concluded that the ONIOM(B3LYP/6-31G(d,p):UFF) scheme is a good method of choice among sophisticated hybrid techniques for investigating many reactions in zeolite catalysts.

LITERATURE CITED

Artioli, G., C. Lamberti, and G. L. Marra. 2000. Neutron powder diffraction study of orthorhombic and monoclinic defective silicalite. **Acta Crystallogr., Sec. B: Structural Science**, B56(1): 2-10.

Atoguchi, T., and S. Yao. 2003. Ti atom in MFI zeolite framework: a large cluster model study by ONIOM method. **J. Mol. Catal. A**, 191(2): 281-288.

Barker, C. M., D. Gleeson, N. Kaltsoyannis, C. R. A. Catlow, G. Sankar, and J. M. Thomas. 2002. On the structure and coordination of the oxygen-donating species in TiMCM-41/TBHP oxidation catalysts: a density functional theory and EXAFS study. **Phys. Chem. Chem. Phys.**, 4(7): 1228-1240.

_____, N. Kaltsoyannis, and C. R. A. Catlow. 2001. A mechanistic exploration of alkene epoxidation mediated by H_2O_2 within porous titanosilicate catalysts. **Stud. Surf. Sci. Catal.**, 135: 2580-2587.

Bellussi, G., A. Carati, M. G. Clerici, G. Maddinelli, and R. Millini. 1992. Reactions of titanium silicalite with protic molecules and hydrogen peroxide. **J. Catal.**, 133(1): 220-230.

_____, and V. Fattore. 1991. Isomorphous substitution in zeolites: a route for the preparation of novel catalysts. **Stud. Surf. Sci. Catal.**, 69: 79-92.

Bengoa, J. F., N. G. Gallegos, S. G. Marchetti, A. M. Alvarez, M. V. Cagnoli, and A. A. Yeramian. 1998. Influence of TS-1 structural properties and operation conditions on benzene catalytic oxidation with H_2O_2. **Micropor. Mesopor. Mater.**, 24(4-6): 163-172.

Bobuatong, K., and J. Limtrakul. 2003. Effects of the zeolite framework on the adsorption of ethylene and benzene on alkali-exchanged zeolites: an ONIOM study. **Appl. Catal. A**, 253(1): 49-64.

Boccuti, M., R., K. M. Rao, A. Zecchina, G. Leofanti, and G. Petrini. 1989. Spectroscopic characterization of silicalite and titanium-silicalite. **Stud. Surf. Sci. Catal.**, 48: 133-144.

Bonino, F., A. Damin, G. Ricchiardi, M. Ricci, G. Spano, R. D'Aloisio, A. Zecchina, C. Lamberti, C. Prestipino, and S. Bordiga. 2004. Ti-peroxo species in the TS-1/H_2O_2/H_2O system. **J. Phys. Chem. B**, 108(11): 3573-3583.

Bordiga, S., S. Coluccia, C. Lamberti, L. Marchese, A. Zecchina, F. Boscherini, F. Buffa, F. Genoni, G. Leofanti, and et al. 1994. XAFS study of Ti-silicalite: Structure of framework Ti(IV) in the presence and absence of reactive

molecules (H_2O, NH_3) and comparison with Ultraviolet-Visible and IR results. **J. Phys. Chem.**, 98(15): 4125-4132.

_____, _____, F. Bonino, G. Ricchiardi, A. Zecchina, R. Tagliapietra, and C. Lamberti. 2003. Resonance Raman effects in TS-1: the structure of Ti(IV) species and reactivity towards H_2O, NH_3 and H_2O_2: an in situ study. **Phys. Chem. Chem. Phys.**, 5(20): 4390-4393.

_____, _____, _____, A. Zecchina, G. Spano, F. Rivetti, V. Bolis, C. Prestipino, and C. Lamberti. 2002. Effect of Interaction with H_2O and NH_3 on the vibrational, electronic, and energetic peculiarities of Ti(IV) centers TS-1 catalysts: A spectroscopic and computational study. **J. Phys. Chem. B**, 106(38): 9892-9905.

Boronat, M., P. M. Viruela, and A. Corma. 2004. Reaction intermediates in acid catalysis by zeolites: Prediction of the relative tendency to form alkoxides or carbocations as a function of hydrocarbon nature and active site structure. **J. Am. Chem. Soc.**, 126(10): 3300-3309.

Clerici, M. G., G. Bellussi, and U. Romano. 1991. Synthesis of propylene oxide from propylene and hydrogen peroxide catalyzed by titanium silicalite. **J. Catal.**, 129(1): 159-167.

Damin, A., S. Bordiga, A. Zecchina, and C. Lamberti. 2002. Reactivity of Ti(IV) sites in Ti-zeolites: An embedded cluster approach. **J. Chem. Phys.**, 117(1): 226-237.

Davis, R. J., Z. Liu, J. E. Tabora, and W. S. Wieland. 1995. X-ray absorption spectroscopy of Ti-containing molecular sieves ETS-10, aluminum-free Ti-b, and TS-1. **Catal. Lett.**, 34(1,2): 101-113.

Dungsrikaew, V., J. Limtrakul, K. Hermansson, and M. Probst. 2003. Comparison of methods for point-charge representation of electrostatic fields. **Int. J. Quantum Chem.**, 96: 17-22.

Feixue, G., Y. Toshihiro, and S. Hideo. 2002. H_2O_2-based epoxidation of bridged cyclic alkenes with $[P\{Ti(O_2)\}_2W_{10}O_{38}]^{7-}$ in monophasic systems: active site and kinetics. **J. Mol. Catal. A**, 180(1-2): 97-108.

Greatbanks, S. P., I. H. Hillier, N. A. Burton, and P. Sherwood. 1996. Adsorption of water and methanol on zeolite Broensted acid sites: an *ab initio*, embedded cluster study including electron correlation. **J. Chem. Phys.**, 105(9): 3370-3776.

Hay, P. J., and W. R. Wadt. 1985. Ab initio effective core potentials for molecular calculations. Potentials for potassium to gold including the outermost core orbitals. **J. Chem. Phys.**, 82: 299-310.

Henry, P. F., M. T. Weller, and C. C. Wilson. 2001. Structural investigation of TS-1: Determination of the true nonrandom titanium framework substitution and silicon vacancy distribution from powder neutron diffraction studies using isotopes. **J. Phys. Chem. B**, 105(31): 7452-7458.

Hijar, C. A., R. M. Jacubinas, J. Eckert, N. J. Henson, P. J. Hay, and K. C. Ott. 2000. The siting of Ti in TS-1 is non-random. powder neutron diffraction studies and theoretical calculations of TS-1 and FeS-1. **J. Phys. Chem. B**, 104(51): 12157-12164.

Hillier, I. H. 1999. Chemical reactivity studied by hybrid QM/MM methods. **J. Mol. Struct. (Theochem)**, 463(1-2): 45-52.

Jeanvoine, Y., and J. G. Angyan. 1998. Bronsted acid sites in HSAPO-34 and Chabazite: An *ab Initio* structural study. **J. Phys. Chem. B**, 102(29): 5573-5580.

Jiang, N., S. Yuan, J. Wang, H. Jiao, Z. Qin, and Y.-W. Li. 2004. A theoretical study of amines adsorption in HMOR by using ONIOM2 method. **J. Mol. Catal. A**, 220(2): 221-228.

Karlsen, E., and K. Schoeffel. 1996. Titanium-silicalite catalyzed epoxidation of ethylene with hydrogen peroxide. A theoretical study. **Catal. Today**, 32: 107-114.

Kasuriya, S., S. Namuangruk, P. Treesukol, M. Tirtowidjojo, and J. Limtrakul. 2003. Adsorption of ethylene, benzene, and ethylbenzene over faujasite zeolites investigated by the ONIOM method. **J. Catal.**, 219(2): 320-328.

Ketrat, S., and J. Limtrakul. 2003. Properties, dynamics, and electronic structure of condensed systems and clusters: Theoretical study of the adsorption of ethylene on alkali-exchanged zeolites. **Int. J. Quantum Chem.**, 94: 333-340.

Khaliullin, R. Z., A. T. Bell, and V. B. Kazansky. 2001. An experimental and density functional theory study of the interactions of CH_4 with H-ZSM-5. **J. Phys. Chem. A**, 105(45): 10454-10461.

Khouw, C. B., C. B. Dartt, J. A. Labinger, and M. E. Davis. 1994. Studies on the catalytic oxidation of alkanes and alkenes by titanium silicates. **J. Catal.**, 149(1): 195-205.

Kumar, R., and A. Bhaumik. 1998. Triphase, solvent-free catalysis over the TS-1/H_2O_2 system in selective oxidation reactions. **Micropor. Mesopor. Mater.**, 21(4-6): 497-504.

Lamberti, C., S. Bordiga, A. Zecchina, G. Artioli, G. Marra, and G. Spano. 2001. Ti location in the MFI framework of Ti-silicalite-1: a neutron powder diffraction study. **J. Am. Chem. Soc.**, 123(10): 2204-2212.

Langhendries, G., D. E. De Vos, G. V. Baron, and P. A. Jacobs. 1999. Quantitative sorption experiments on Ti-zeolites and relation with a-olefin oxidation by H_2O_2. **J. Catal.**, 187(2): 453-463.

Limtrakul, J., C. Inntam, and T. N. Truong. 2004. Density functional theory study of the ethylene epoxidation over Ti-substituted silicalite (TS-1). **J. Mol. Catal. A**, 207(2): 139-148.

_____, S. Jungsuttiwong, and P. Khongpracha. 2000. Adsorption of carbon monoxide on H-FAU and Li-FAU zeolites. An embedded cluster approach. **J. Mol. Struct.**, 525: 153-162.

_____, T. Nanok, S. Jungsuttiwong, P. Khongpracha, and T. N. Truong. 2001a. Adsorption of unsaturated hydrocarbons on zeolites: the effects of the zeolite framework on adsorption properties of ethylene. **Chem. Phys. Lett.**, 349(1-2): 161-166.

_____, S. Nokbin, P. Chuichay, S. Jungsuttiwong, and P. Khongpracha. 2001b. Coverage effects on adsorption of water in faujasite: an ab initio cluster and embedded cluster study. **Stud. Surf. Sci. Catal.**, 135: 2469-2476.

Lin, W., and H. Frei. 2002. Photochemical and FT-IR probing of the active site of hydrogen peroxide in Ti silicalite sieve. **J. Am. Chem. Soc.**, 124(31): 9292-9298.

Mantegazza, M. A., G. Petrini, G. Fornasari, A. Rinaldo, and F. Trifiro. 1996. Ammoximation reaction in the gas and liquid phases with silica based catalysts: role of titanium. **Catal. Today**, 32: 297-304.

_____, G. Petrini, G. Spano, R. Bagatin, and F. Rivetti. 1999. Selective oxidations with hydrogen peroxide and titanium silicalite catalyst. **J. Mol. Catal. A**, 146(1-2): 223-228.

Mimmoun, H., M. Postel, F. Casabianca, J. Fisher, and A. Mitschler. 1982. Novel unusually stable peroxotitanium(IV) compounds. Molecular and crystal structure of peroxobis(picolinato)(hexamethylphosphoric triamide)titanium(IV). **Inorg. Chem.**, 21(4): 1303-1306.

Munakata, H., Y. Oumi, and A. Miyamoto. 2001. A DFT study on peroxo-complex in titanosilicate catalyst: hydrogen peroxide activation on Titanosilicalite-1 catalyst and reaction mechanisms for catalytic olefin epoxidation and for hydroxylamine formation from ammonia. **J. Phys. Chem. B**, 105(17): 3493-3501.

Namuangruk, S., P. Pantu, and J. Limtrakul. 2004. Alkylation of benzene with ethylene over faujasite zeolite investigated by the ONIOM method. **J. Catal.**, 225(2): 523-530.

Panjan, W., and J. Limtrakul. 2003. The influence of the framework on adsorption properties of ethylene/H-ZSM-5 system: an ONIOM study. **J. Mol. Struct.**, 654(1-3): 35-45.

Pei, S., G. W. Zajac, J. A. Kaduk, J. Faber, B. I. Boyanov, D. Duck, D. Fazzini, T. I. Morrison, and D. S. Yang. 1993. Re-investigation of titanium silicalite by x-ray absorption spectroscopy: are the novel titanium sites real? **Catal. Lett.**, 21(3-4): 333-344.

Perego, C., A. Carati, P. Ingallina, M. A. Mantegazza, and G. Bellussi. 2001. Production of titanium containing molecular sieves and their application in catalysis. **Appl. Catal. A**, 221(1-2): 63-72.

Raksakoon, C., and J. Limtrakul. 2003. Adsorption of aromatic hydrocarbon onto H-ZSM-5 zeolite investigated by ONIOM study. **J. Mol. Struct. (Theochem)**, 631: 147-156.

Ricchiardi, G., A. Damin, S. Bordiga, C. Lamberti, and A. Zecchina. 2001. Vibrational structure of titanium silicate catalysts. A spectroscopic and theoretical study. **J. Am. Chem. Soc.**, 123(11409-11419).

Rungsirisakun, R., B. Jansang, P. Pantu, and J. Limtrakul. 2004. The adsorption of benzene on industrially important nanostructured catalysts (H-BEA, H-ZSM-5, and H-FAU): confinement effects. **J. Mol. Struct. (Theochem)**, 733(1-3): 239-246.

Sankar, G., J. M. Thomas, C. R. A. Catlow, C. M. Barker, D. Gleeson, and N. Kaltsoyannis. 2001. The three-dimensional structure of the titanium-centered active site during steady-state catalytic epoxidation of alkenes. **J. Phys. Chem. B**, 105(38): 9028-9030.

Sauer, J., and M. Brandle. 1998. Acidity differences between inorganic solids Induced by their framework structure. A combined Quantum Mechanics/Molecular Mechanics ab Initio study on zeolites. **J. Am. Chem. Soc.**, 120(7): 1556-1570.

_____, and M. Sierka. 2000. Combining quantum mechanics and interatomic potential functions in ab initio studies of extended systems. **J. Comp. Chem.**, 21(16): 1470-1493.

Sever, R. R., and T. W. Root. 2003a. DFT study of solvent coordination effects on titanium-based epoxidation catalysts. Part One: Formation of the titanium hydroperoxo intermediate. **J. Phys. Chem. B**, 107(17): 4080-4089.

_____, and _____. 2003b. DFT study of solvent coordination effects on titanium-based epoxidation catalysts. Part two: Reactivity of titanium hydroperoxo complexes in ethylene epoxidation. **J. Phys. Chem. B**, 107(17): 4090-4099.

Shah, R., J. D. Gale, and M. C. Payne. 1997. Comparing the acidities of zeolites and SAPOs from first principles. **Chem. Commun.**: 131-132.

Sillar, K., and P. Burk. 2004. Computational study of vibrational frequencies of bridging hydroxyl groups in zeolite ZSM-5. **Chem. Phys. Lett.**, 393(4-6): 285-289.

Sinclair, P. E., and C. R. A. Catlow. 1999. Quantum chemical study of the mechanism of partial oxidation reactivity in titanosilicate catalysts: Active site formation, oxygen transfer, and catalyst deactivation. **J. Phys. Chem. B**, 103(7): 1084-1095.

_____, G. Sankar, C. R. A. Catlow, J. M. Thomas, and T. Maschmeyer. 1997. Computational and EXAFS study of the nature of the Ti(IV) active sites in mesoporous titanosilicate catalysts. **J. Phys. Chem. B**, 101(21): 4232-4237.

_____, A. d. Vries, P. Sherwood, C. R. A. Catlow, and R. A. van Santen. 1998. Quantum-chemical studies of alkene chemisorption in chabazite: A comparison of cluster and embedded-cluster models. **J. Chem. Soc., Faraday Trans.**, 94: 3401-3408.

Solans-Monfort, X., J. Bertran, V. Branchadell, and M. Sodupe. 2002. Keto-Enol isomerization of acetaldehyde in HZSM-5. A theoretical study using the ONIOM2 method. **J. Phys. Chem. B**, 106(39): 10220-10226.

_____, M. Sodupe, V. Branchadell, J. Sauer, R. Orlando, and P. Ugliengo. 2005. Adsorption of NH_3 and H_2O in acidic chabazite. Comparison of ONIOM approach with periodic calculations. **J. Phys. Chem. B**, 109(8): 3539-3545.

Svensson, M., S. Humbel, R. D. J. Froese, T. Matsubara, S. Sieber, and K. Morokuma. 1996. ONIOM: A multi-layered integrated MO + MM method for geometry optimizations and single point energy predictions. A test for diels-alder reactions and $Pt(P(t-Bu)_3)_2 + H_2$ oxidative addition. **J. Phys. Chem.**, 100(50): 19357-19363.

Tantanak, D., M. A. Vincent, and I. H. Hillier. 1998. Elucidation of the mechanism of alkene epoxidation by hydrogen peroxide catalyzed by titanosilicates: a computational study. **Chem. Commun.**(9): 1031-1032.

Taramasso, M., G. Perego, and B. Notari. 1983. **Preparation of porous crystalline synthetic material comprised of silicon and titanium oxides.** U.S. Patent 4410501.

Teunissen, E. H., A. P. J. Jansen, and R. A. van Santen. 1994. Adsorption energies of NH$_3$ and NH$_4^+$ in zeolites corrected for the long-range electrostatic potential of the crystal. **J. Chem. Phys.**, 101(7): 5865-5874.

Tozzola, G., M. A. Mantegazza, G. Ranghino, G. Petrini, S. Bordiga, G. Ricchiardi, C. Lamberti, R. Zulian, and A. Zecchina. 1998. On the structure of the active site of Ti-Silicalite in reactions with hydrogen peroxide: a vibrational and computational study. **J. Catal.**, 179(1): 64-71.

Treesukol, P., J. Limtrakul, and T. N. Truong. 2001. Adsorption of nitrogen monoxide and carbon monoxide on copper-exchanged ZSM-5: A cluster and embedded cluster study. **J. Phys. Chem. B**, 105(12): 2421-2428.

van der Pol, A. J. H. P., and J. H. C. van Hooff. 1993. Oxidation of linear alcohols with hydrogen peroxide over titanium silicalite 1. **Appl. Catal. A**, 106(1): 97-113.

Van Koningsveld, H., H. Van Bekkum, and J. C. Jansen. 1987. On the location and disorder of the tetrapropylammonium (TPA) ion in zeolite ZSM-5 with improved framework accuracy. **Acta Crystallogr., Sec. B: Structural Science**, B43(2): 127-132.

Van Santen, R. A., and G. J. Kramer. 1995. Reactivity theory of zeolitic bronsted acidic sites. **Chem. Rev.**, 95: 637-660.

Vayssilov, G. N., and R. A. Van Santen. 1998. Catalytic activity of titanium silicalites - a DFT study. **J. Catal.**, 175(2): 170-174.

Wells, D. H., Jr., W. N. Delgass, and K. T. Thomson. 2004. Evidence of defect-promoted reactivity for epoxidation of propylene in titanosilicate (TS-1) catalysts: a DFT study. **J. Am. Chem. Soc.**, 126(9): 2956-2962.

Yamase, T., E. Ishikawa, Y. Asai, and S. Kanai. 1996. Alkene epoxidation by hydrogen peroxide in the presence of titanium-substituted Keggin-type polyoxotungstates $[PTi_xW_{12-x}O_{40}]^{(3+2x)-}$ and $[PTi_xW_{12-x}O_{40-x}(O_2)_x]^{(3+2x)-}$ (x = 1 and 2). **J. Mol. Catal. A**, 114(1-3): 237-245.

Yudanov, I. V., P. Gisdakis, C. Di Valentin, and N. Rosch. 1999. Activity of peroxo and hydroperoxo complexes of Ti(IV) in olefin epoxidation. A density functional model study of energetics and mechanism. **Eur. J. Inorg. Chem.**(12): 2135-2145.

Zecchina, A., S. Bordiga, C. Lamberti, G. Ricchiardi, D. Scarano, G. Petrini, G. Leofanti, and et al. 1996. Structural characterization of Ti centers in Ti-silicalite and reaction mechanisms in cyclohexanone ammoximation. **Catal. Today**, 32: 97-106.

Zhuang, J., D. Ma, Z. Yan, F. Deng, X. Liu, X. Han, X. Bao, X. W. Liu, X. Guo, and X. Wang. 2004. Solid-state MAS NMR detection of the oxidation center in TS-1 zeolite by in situ probe reaction. **J. Catal.**, 221(2): 670-673.

CURRICULUM VITAE

NAME	:	Mr. Weerayuth Panyaburapa
BIRTH DATE	:	November 21, 1978.
BIRTH PLACE	:	Bangkok, Thailand

EDUCATION :

YEAR	**INSTITUTION**	**DEGREE/DIPLOMA**
2000	Kasetsart Univ.	B.S. (Chemistry)

SCHOLASHIP : Ministry of University Affairs under the Science and Technology Higher Education Development project (MUA-ADB funds)

Teaching Assistance, Physical chemistry Division, Kasetsart University

PRESENTATION

Panyaburapa, W., J. Limtrakul. **The partial oxidation of unsaturated hydrocarbons with H_2O_2 over TS-1 investigated by the ONIOM method: formation of active site and reaction mechanism**. 31st Congress in Science and Technology of Thailand, October, 2005. Nakhonratchasima, Thailand.